



Calhoun: The NPS Institutional Archive DSpace Repository

Theses and Dissertations

1. Thesis and Dissertation Collection, all items

1989-03

A numerical study of a mesoscale eddy interaction with an ocean front in the marginal ice zone

Lumpkin, Rutledge P.

Monterey, California. Naval Postgraduate School

<http://hdl.handle.net/10945/26114>

Downloaded from NPS Archive: Calhoun



<http://www.nps.edu/library>

Calhoun is the Naval Postgraduate School's public access digital repository for research materials and institutional publications created by the NPS community.

Calhoun is named for Professor of Mathematics Guy K. Calhoun, NPS's first appointed -- and published -- scholarly author.

Dudley Knox Library / Naval Postgraduate School
411 Dyer Road / 1 University Circle
Monterey, California USA 93943



NAVAL POSTGRADUATE SCHOOL

Monterey, California



THESIS

18953

A NUMERICAL STUDY OF A MESOSCALE
EDDY INTERACTION WITH AN OCEAN FRONT
IN THE MARGINAL ICE ZONE

by

Rutledge P. Lumpkin

March 1989

Thesis advisor

D.C. Smith, IV

Approved for public release; distribution is unlimited

T242057

UNCLASSIFIED

SECURITY CLASSIFICATION OF THIS PAGE

REPORT DOCUMENTATION PAGE

REPORT SECURITY CLASSIFICATION UNCLASSIFIED		1b RESTRICTIVE MARKINGS					
SECURITY CLASSIFICATION AUTHORITY		3 DISTRIBUTION / AVAILABILITY OF REPORT Approved for public release, distribution is unlimited					
DECLASSIFICATION / DOWNGRADING SCHEDULE							
PERFORMING ORGANIZATION REPORT NUMBER(S)		5 MONITORING ORGANIZATION REPORT NUMBER(S)					
NAME OF PERFORMING ORGANIZATION Naval Postgraduate School	6b OFFICE SYMBOL (If applicable) 68	7a NAME OF MONITORING ORGANIZATION Naval Postgraduate School					
ADDRESS (City, State, and ZIP Code) Monterey, California 93943-5000		7b ADDRESS (City, State, and ZIP Code) Monterey, CA 93943-5000					
NAME OF FUNDING SPONSORING ORGANIZATION	8b OFFICE SYMBOL (If applicable)	9 PROCUREMENT INSTRUMENT IDENTIFICATION NUMBER					
ADDRESS (City, State and Zip Code)		10 SOURCE OF FUNDING NUMBERS <table border="1"> <tr> <td>PROGRAM ELEMENT NO</td> <td>PROJECT NO</td> <td>TASK NO</td> <td>WORK UNIT ACCESSION NO</td> </tr> </table>		PROGRAM ELEMENT NO	PROJECT NO	TASK NO	WORK UNIT ACCESSION NO
PROGRAM ELEMENT NO	PROJECT NO	TASK NO	WORK UNIT ACCESSION NO				
TITLE (Include Security Classification) NUMERICAL STUDY OF A MESOSCALE EDDY INTERACTION WITH AN OCEAN FRONT IN THE MARGINAL ICE ZONE							
PERSONAL AUTHOR(S) Pumpkin, Rutledge P.							
TYPE OF REPORT Master's Thesis	13b TIME COVERED FROM _____ TO _____	14 DATE OF REPORT (Year, Month Day) 1989 March	15 PAGE COUNT 98				
SUPPLEMENTARY NOTATION The views expressed in this thesis are those of the author and do not reflect the policy of the Dept. of Defense or the U.S. Navy.							
COSATI CODES		16 SUBJECT TERMS (Continue on reverse if necessary and identify by block number) Eddy-Jet Interaction, Numerical Simulations					
ABSTRACT (Continue on reverse if necessary and identify by block number) The East Greenland Current and its associated Marginal Ice Zone is a region of intense nodynamical activity. A two layer, primitive equation, numerical model is used to simulate an eddy-jet interaction in the East Greenland marginal ice zone region. The effects of wind direction, topography, and sense of eddy rotation on the eddy-jet interaction are examined to determine the seaward ice transport, icebanding, and dipole formation. It is determined that an anticyclone (15 cm/s) interaction with a jet (30 cm/s) will develop a dipole that advects ice away from the ice edge. This phenomenon is not observed for a cyclone-jet interaction. It is also seen that a jet with no winds flowing parallel to the ice edge will create an iceband due to the cross ice edge Ekman transport. The interaction of both the cyclone and anticyclone with the jet creates downstream perturbations in the jet leading to a sinuous ice edge. Winds greater than 10 m/s dominate the ice dynamics over that induced by the ocean flow fields.							
DISTRIBUTION/AVAILABILITY OF ABSTRACT <input checked="" type="checkbox"/> UNCLASSIFIED/UNLIMITED <input type="checkbox"/> SAME AS PPT <input type="checkbox"/> C USERS		21 ABSTRACT SECURITY CLASSIFICATION unclassified					
22 NAME OF RESPONSIBLE INDIVIDUAL D. C. Smith, IV		22b TELEPHONE (Include Area Code) (408) 646-3350	22c OFFICE SYMBOL 68Si				

G FORM 1473, R4MA.

83 APPENDIXES MAY BE USED UNTIL EXHAUSTED

All other editions are obsolete

SECURITY CLASSIFICATION OF THIS PAGE

U. S. Government Printing Office 1986-606-243

Approved for public release; distribution is unlimited

A Numerical Study of a Mesoscale Eddy Interaction
with an Ocean Front in the Marginal Ice Zone

by

Rutledge P. Lumpkin
Lieutenant, United States Navy
B.S., University of South Carolina, 1979

Submitted in partial fulfillment of the
requirements for the degree of

MASTER OF SCIENCE IN METEOROLOGY AND OCEANOGRAPHY

from the

NAVAL POSTGRADUATE SCHOOL
March 1989

ABSTRACT

The East Greenland Current and its associated Marginal Ice Zone is a region of intense dynamical activity. A two layer, primitive equation, numerical model is used to simulate an eddy-jet interaction in the East Greenland marginal ice zone region. The effects of wind direction, topography, and sense of eddy rotation on the eddy-jet interaction are examined to determine the seaward ice transport, icebanding, and dipole formation. It is determined that an anticyclone (15 cm/s) interacting with a jet (30 cm/s) will develop a dipole that advects ice away from the ice edge. The dipole formation and ice advection away from the ice edge is not seen for a cyclone-jet interaction. It is also seen that a jet with no winds flowing parallel to the ice edge will create an iceband due to the cross ice edge Ekman transport. The interaction of both the cyclone and anticyclone with the jet creates downstream perturbations in the jet leading to a sinuous ice edge. Winds greater than 10 m/s dominate the ice dynamics over that induced by the ocean flow fields.

Thesis
L8753
C.1

TABLE OF CONTENTS

I.	INTRODUCTION	1
	A. THE EAST GREENLAND CURRENT REGION	1
	B. EDDY CHARACTERISTICS	2
	C. PURPOSE	5
II.	PREVIOUS WORK	10
	A. UPWELLING/DOWNWELLING	10
	B. OPEN OCEAN EDDY INTERACTION WITH THE MIZ	11
	C. EDDY JET INTERACTION	16
	D. ICEBANDING	19
III.	NUMERICAL TECHNIQUE AND MODEL PARAMETERS	21
	A. THE OCEAN MODEL	22
	B. BOUNDARY AND INITIAL CONDITIONS	24
	C. THE ICE MODEL	28
	D. WIND FORCING	32
IV.	EXPERIMENTS	33
	A. PURPOSE OF EXPERIMENTS	33
	B. PRELIMINARY EXPERIMENTS	33
	1. Simulations with No Wind	34
	a. Experiment 1A	34

2.	Simulation with Wind	36
a.	Experiment 1B	37
C.	PRIMARY EXPERIMENTS	47
1.	Experiment 2A.	47
2.	Experiment 2B.	50
3.	Experiment 3A	51
4.	Experiment 3B	54
5.	Experiment 4A	54
6.	Experiment 4B	56
7.	Topography.	74
V.	CONCLUSIONS	75
VI.	RECOMMENDATIONS	79
APPENDIX: SYMBOLS AND NOTATION		80
LIST OF REFERENCES		82
INITIAL DISTRIBUTION LIST		84

LIST OF TABLES

Table 1. Summary of Experiments	34
---	----

LIST OF FIGURES

Figure 1.1	Fram Strait Circulation	6
Figure 1.2	MIZ Ice Edge Eddy	7
Figure 1.3	Schematic Ice Edge-Eddy Interaction Observed during MIZEX 84	8
Figure 1.4	Lagrangian Surface Drifters	9
Figure 2.1	Ekman Induced Upwelling	13
Figure 2.2	Wind Forced Upwelling/Downwelling in Sinuous Ice Edge	14
Figure 2.3	Vorticity Input into Upper Ocean by Along Ice Edge Winds	15
Figure 2.4	Eddy-Jet Interaction	18
Figure 3.1	Coupled Ice Model	30
Figure 3.2	Ekman Divergence in Ice Concentration.	31
Figure 4.1	Mean Wind Direction and Speed	40
Figure 4.2	Ice Concentration Day 1, 2, & 4, JET-ICE Edge with No Wind Exp 1A	41
Figure 4.3	\mathbf{u} Velocity and Ice Concentration Across MIZ, Day 1 Exp 1A	42
Figure 4.4	\mathbf{u} Velocity and Ice Concentration Across MIZ, Day 2 Exp 1A	43
Figure 4.5	\mathbf{u} Velocity and Ice Concentration Across MIZ, Day 4 Exp 1A	44

Figure 4.6	u Velocity and Ice Concentration Across MIZ, Day 4 Exp 1B	45
Figure 4.7	Interfacial Height Anomaly Day 6 Exp 1B	46
Figure 4.8	Upper Level Relative Vorticity Day 0-6	57
Figure 4.9	Ice Concentration Day 1, 2, 4, 6	58
Figure 4.10	Synthetic Aperture Radar Imagery MIZEX 1987	59
Figure 4.11	Upper Level Relative Vorticity Day 1, 2, 4, 6 Exp 2B	60
Figure 4.12	Ice Concentration for Day 1-6 Exp 2B	61
Figure 4.13	Upper Level Relative Vorticity Day 1-6 Exp 3A	62
Figure 4.14	Relative Vorticity in the Lower Level Day 6 Exp 3A	63
Figure 4.15A	Velocity Vectors and Isotachs at the Surface Day 6 Exp 1A	64
Figure 4.15B	Velocity Vectors and Isotachs at the Surface Day 6 Exp 3A	64
Figure 4.16	Ice Concentration for Day 1-6 Exp 3A	65
Figure 4.17	Interfacial Height Anomaly Day 6 Exp 3A	66
Figure 4.18	x-t Plot of Pynocline Height Anomaly	66
Figure 4.19A	Relative Vorticity in the Upper Layer Across the MIZ Exp 1A	67
Figure 4.19B	Relative Vorticity in the Upper Layer Across the MIZ Exp 2A	68
Figure 4.20	Height Anomaly in the Upper Level, Day 0.5-2.5 Exp 3B	69

Figure 4.21	Ice Concentration Day 1-6 Exp 4A . . .	70
Figure 4.22	Interfacial Height Anomaly Day 2, 4 & 6 Exp 4A	71
Figure 4.23	Upper Level Relative Vorticity Day 1-6 Exp 4A	72
Figure 4.24	Ice Concentration Day 1-2 Exp 4B . . .	73

I. INTRODUCTION

A. THE EAST GREENLAND CURRENT REGION

The East Greenland Current and its associated marginal ice zone (MIZ) is a region of intense dynamical activity with complex mesoscale ocean processes influencing the ice edge. Figure 1.1, from Paquette et al. (1985) shows the general circulation of the region. Since the Fram Strait region is the primary source for Atlantic Water flowing into the Arctic basin and Polar water flowing out of the Arctic Basin, the region's importance both tactically and scientifically is striking. Experiments such as the Marginal Ice Zone Experiment (MIZEX), have been conducted this decade using shipboard sensors, Lagrangian drifters, and satellite imagery. From the results of these studies, an understanding of the mesoscale dynamics of the oceanographic phenomena is beginning to evolve. Figure 1.2 is a remarkable photograph of a cyclonic eddy/ice edge interaction in the marginal ice zone. The marginal ice zone is divided into two different regions of ice concentration, Gascard et al. (1988). The outermost region,

along the ice ocean interface, is delineated by a sinuous edge with an ice concentration of 3/10 or less. The inner region is defined by an ice concentration of 4/10 or greater. Gascard et al. (1988) summarizes the MIZ as an area of low ice concentration, typical floe sizes ranging from one to 25 km, and variable eddy features located between these two limits.

B. EDDY CHARACTERISTICS

A number of mechanisms, five of which were proposed by Johannessen et al. (1987), may be responsible for the generation of the observed mesoscale eddies. Among the generation mechanisms are barotropic and baroclinic instability of the East Greenland Current or marginal ice edge front, differential Ekman pumping along the ice edge, topographic generation, and ice edge instability driven by internal ice dynamics. Johannessen et al. (1983) documented a 10 km wide ice edge mesoscale ocean front in the East Greenland Current. The jet front was located in 4000 meters of water with velocities of 10 cm/s. Several mesoscale eddies with length scales ranging from 5 to 15 km were also documented. Both the jet and the eddies exhibited little vertical shear. Based on observations

and theory, Johannessen et al. (1983) concluded that the eddies resulted from barotropic instability of the oceanic front. The energy derived by the eddies came from the kinetic energy of the mean flow. Figure 1.3 from Johannessen et al. (1987) depicts schematically the interaction of an open ocean mesoscale eddy with the ice edge.

According to Gascard et al. (1988), from observations during the 1983 and 1984 marginal ice zone experiment, the East Greenland Current (EGC) is a narrow, stable current. Gascard et al. (1988) suggested that the West Spitzbergen Current (WSC) and the Norwegian current are the main generators of mesoscale eddies in the Fram Strait. The eddies are then advected by the return Atlantic flow following bathymetric fracture zones into the East Greenland Current. Foldvik et al. (1988) support this argument by concluding the lateral turbulent heat flux associated with the East Greenland Current is insufficient to be consistent with local generation of eddies through baroclinic instability.

Using Lagrangian drifters, Gascard et al. (1988) traced this eddy path and documented the interaction of open ocean

eddies with the ice edge and the East Greenland ocean front (Figure 1.4). While some of the eddies were anticyclonic, the majority were cyclonic, consistent with the earlier findings of Johannessen (1983). Because the East Greenland Current follows closely the continental slope of East Greenland, topography may also be important in the interaction of the eddies with the East Greenland Current and the MIZ.

Wind forcing has been shown to cause upwelling and downwelling at the ice edge. Hakkinen (1986b) showed how winds parallel to the ice edge with the ice edge on the right would produce upwelling. Conversely, a wind with the ice edge to the left would produce downwelling in the pycnocline. Wind at the ice edge can also result in vorticity input into the ocean. This is demonstrated in Smith et al. (1988) where upwelling favorable winds were shown to destroy ocean anticyclones at the ice edge. Along ice edge winds may thus also be important in the interaction of eddies with the East Greenland Current marginal ice zone. These processes will be discussed in further detail in the next section.

C. PURPOSE

In this study, the interaction of an open ocean eddy with a marginal ice zone and associated along ice edge ocean front is considered. Results are obtained using a coupled air-ice-ocean numerical model. The effects of winds and topography on the eddy interaction with the MIZ and the East Greenland ocean front are included.

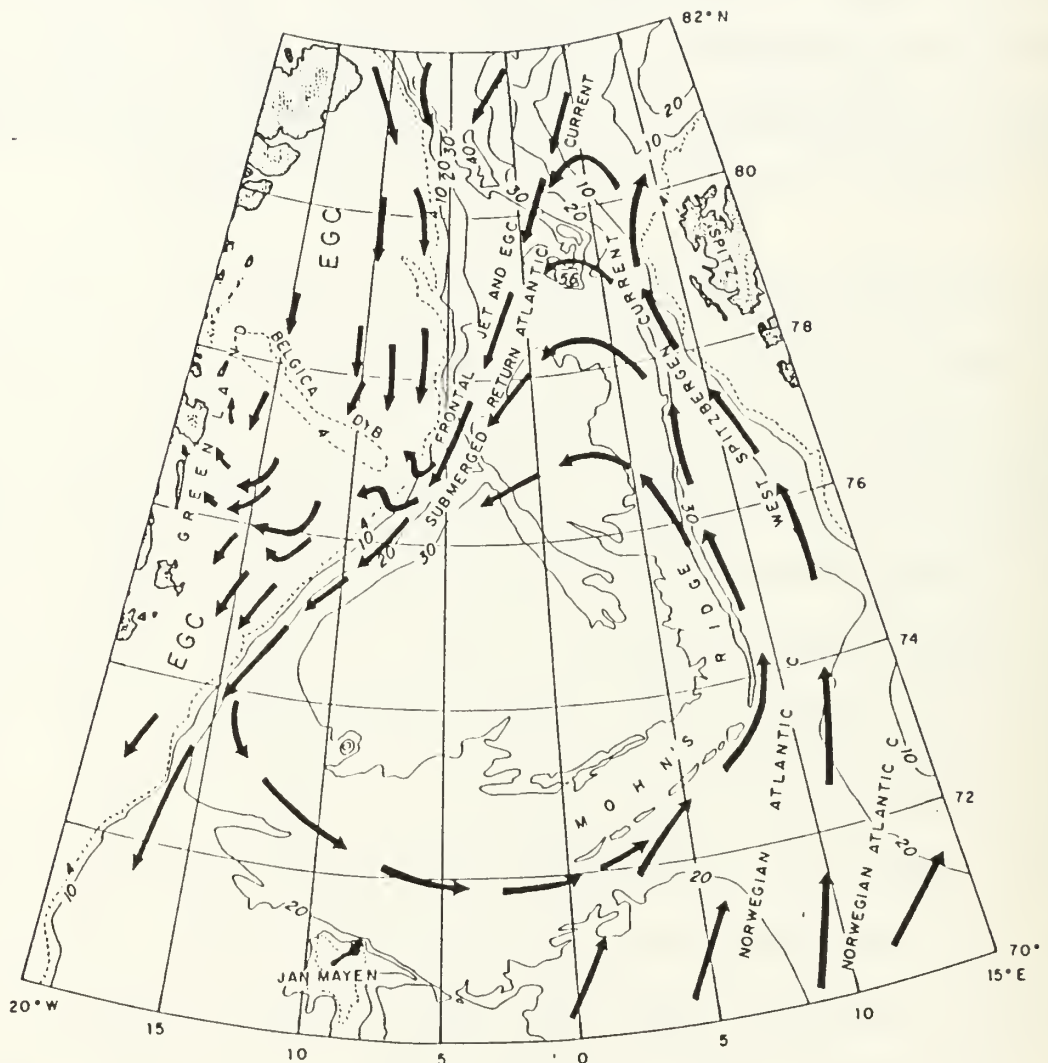


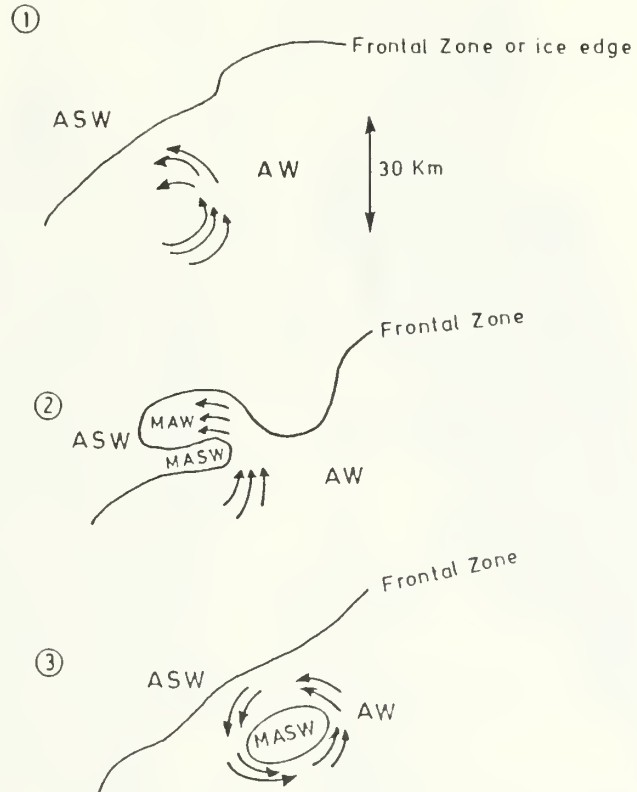
Figure 1.1 Fram Strait Circulation

Source: Paquette et al. (1985)



Figure 1.2 MIZ Ice Edge Cyclonic Eddy

Source: Johannessen et al. (1987)



AW - Atlantic Water
 ASW - Arctic Surface Water
 MAW - Modified Atlantic Water
 MASW - Modified Arctic Surface Water

Figure 1.3 Schematic Ice Edge- Eddy Interaction
Observed During MIZEX 84

Source: Johannessen et al. (1987)

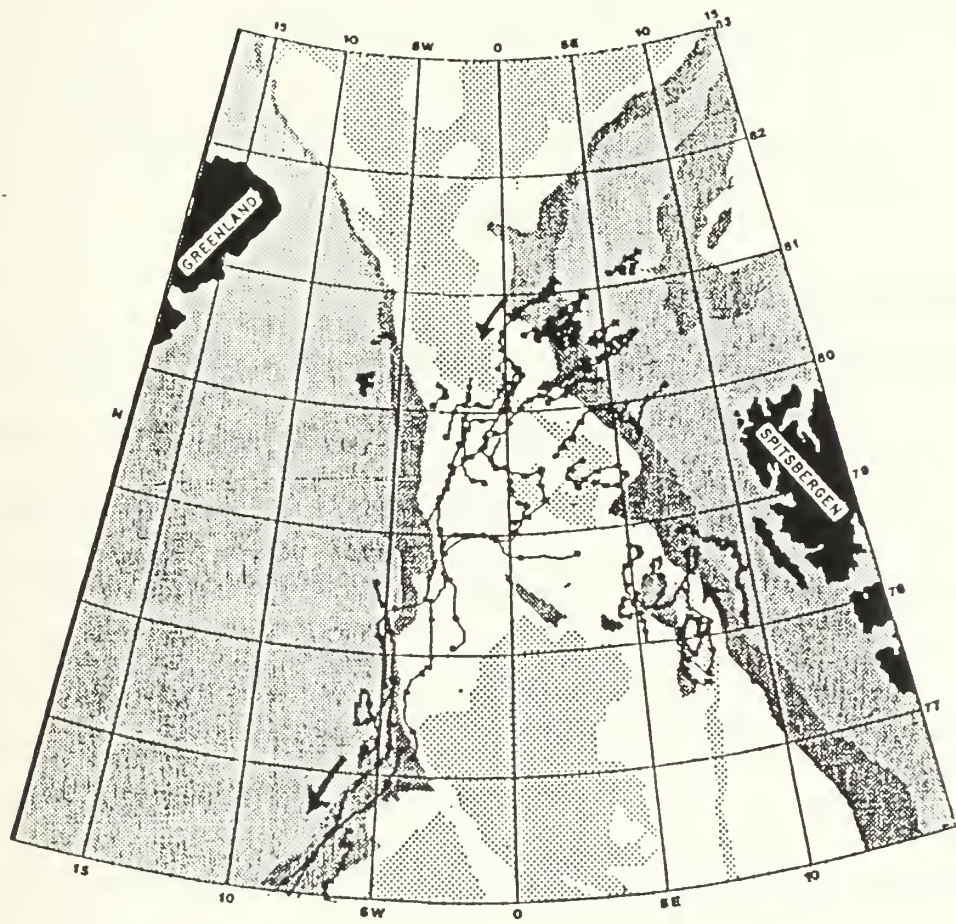


Figure 1.4 Lagrangian Surface Drifter Trajectories
Indicating Eddy Trajectories across Fram
strait (Dots represent 0000 UT on each
day)

Source: Gascard et al. (1988)

II. PREVIOUS WORK

Numerous mesoscale physical processes have been identified as important in the MIZ region. A brief description of previous findings will facilitate explanation of results in this study.

A. UPWELLING/DOWNWELLING

Winds varying with time have distinct dynamical effects on the ice edge. Hakkinen (1986b) showed how winds parallel to the ice edge, with the ice edge on the right, would produce upwelling. The momentum flux of the air to the ocean is smaller than the momentum flux from the air to ice to ocean so continuity dictates upwelling in the pycnocline, Figure 2.1. The opposite holds true for a wind with the ice edge to the left and there would be a downwelling band. With the assumption of a sinuous ice edge, Hakkinen (1986b) showed how Ekman pumping drives both upwelling and downwelling along the ice edge, Figure 2.2. It is also demonstrated how eddies are formed at the ice edge through differential Ekman pumping. This study will show how a sinuous ice edge can occur from the

interaction of a cyclonic or anticyclonic eddy and a stable barotropic jet.

B. OPEN OCEAN EDDY INTERACTION WITH THE MIZ

Smith et al. (1988) showed that at high latitudes an eddy decays much more slowly than at lower latitudes. This is because the westward propagation speed of the eddy is limited to the Rossby long wave speed, $c = -\beta R_d^2$, where c is the wave speed, β is the planetary vorticity gradient, and R_d is the Rossby radius of deformation. At 80°N , the Rossby long wave speed (c) is on the order of .01 km/day, so the decay time associated with the Rossby wave radiation takes much longer. Since the simulations in this study are limited to periods of less than six days, the observed eddy motion and decay are not due to Rossby wave dynamics.

The interaction of a mesoscale open ocean eddy with a marginal ice zone in the absence of an along ice edge ocean front is considered in Smith et al. (1988). They determined that the Coriolis term in the ice momentum equations, without ocean surface slope terms, caused divergence of the ice over a cyclone and convergence of the ice over an anticyclone. When the pressure force in

the ice caused by the ocean slope is included in the ice momentum equations, a geostrophic balance occurs in the ice. This means that the pressure gradient force is as important as the Coriolis force and should be included in the equations of motion. The geostrophic balance holds true for a light wind situation only. When winds are greater than 10 m/s, the geostrophic balance becomes secondary and the wind forcing dominates. Smith et al. (1988) also demonstrated that upwelling winds provide cyclonic vorticity to the ocean destroying anticyclonic eddies (see Figure 2.3). Similarly, downwelling winds provide anticyclonic vorticity which destroys cyclonic eddies. They also suggested that since 12 of the 14 eddies observed by Johannessen et al. (1987) were cyclonic eddies, the upwelling winds during MIZEX-84, destroyed the anticyclonic eddies. In this study, both upwelling and downwelling winds will be examined.

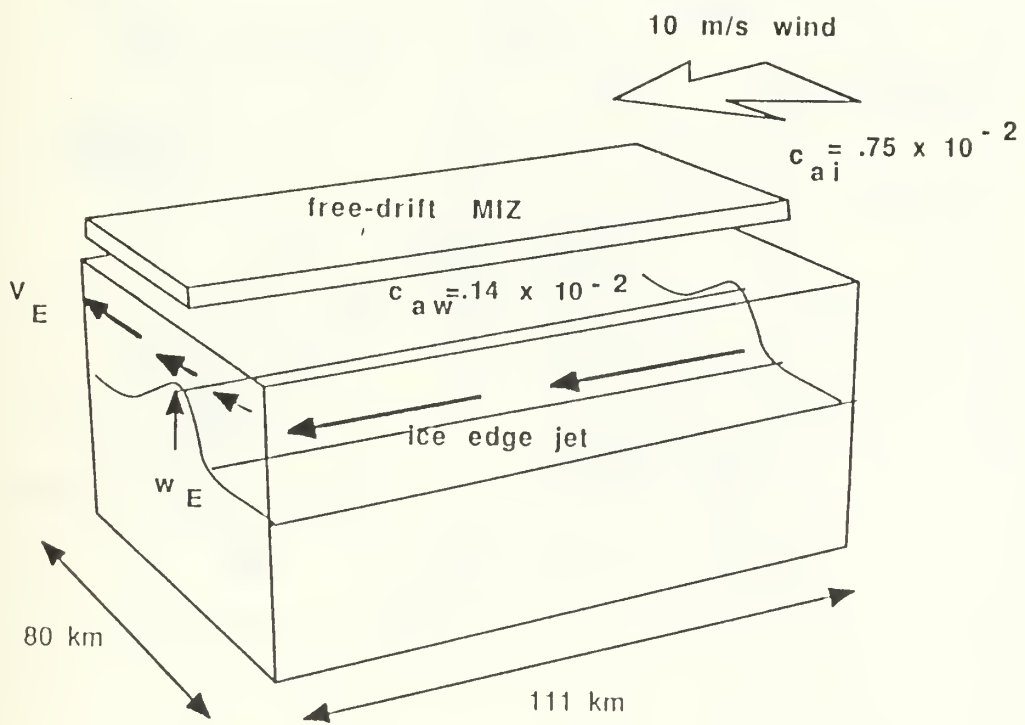
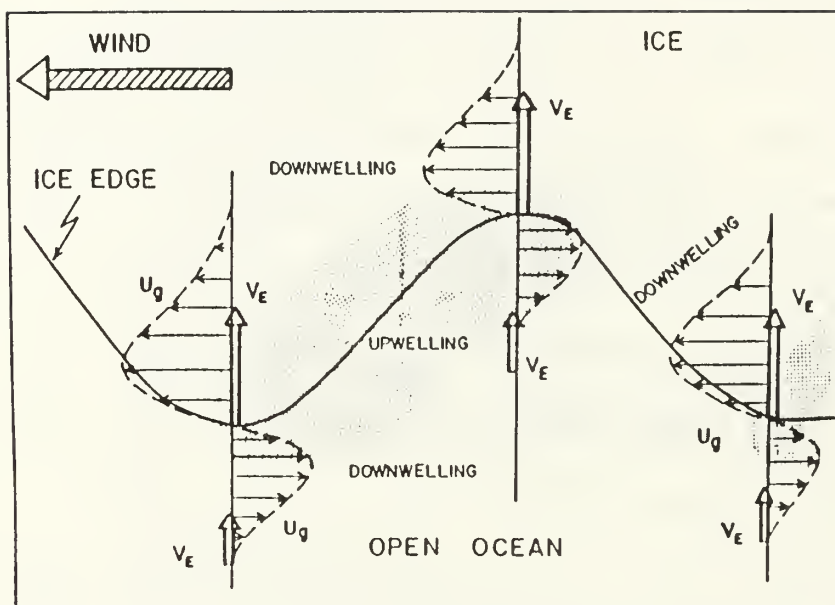


Figure 2.1 Ekman Induced Upwelling (W_F) by Along Ice Edge Winds (symbols defined in Appendix)



V_E - Ekman induced cross ice flow
 U_g - Geostrophically balanced along ice edge jet

Figure 2.2 Wind Forced Upwelling/Downwelling in a Sinuous Ice Edge

Source: Hakkinen (1986b)

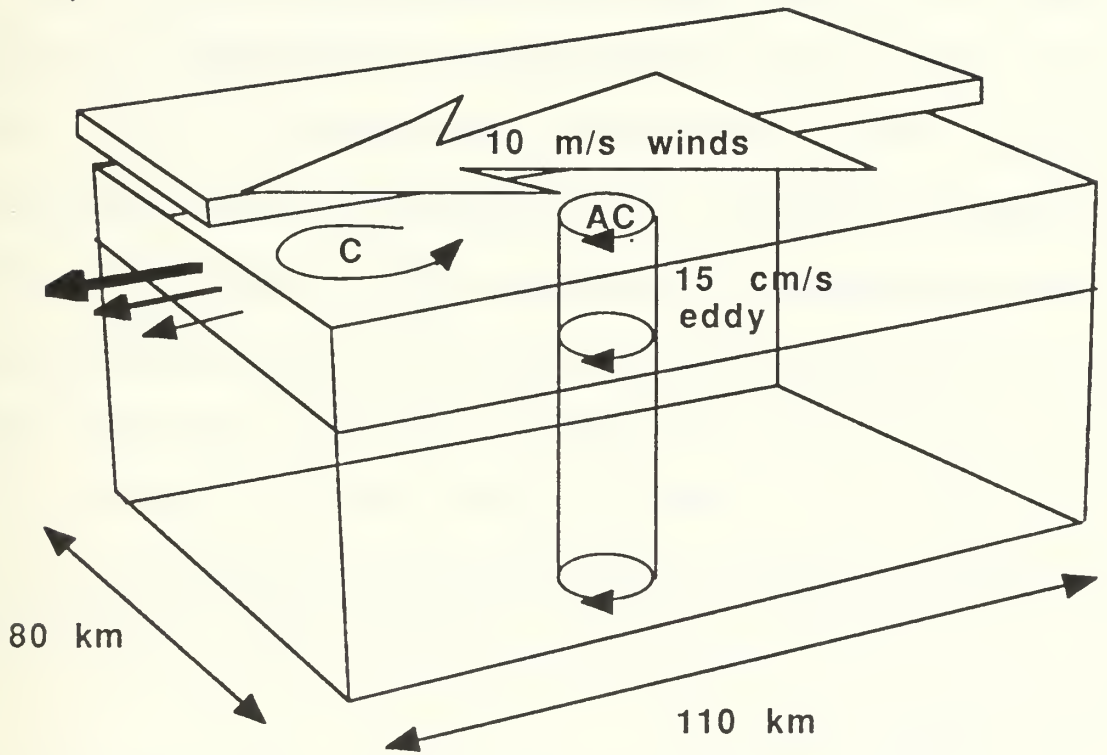


Figure 2.3 Cyclonic Vorticity Input to Upper Ocean by Along Ice Edge Winds (AC denotes existing ocean anticyclone)

C. EDDY JET INTERACTION

The interaction of an eddy with an ocean jet in the absence of ice was first examined by Stern and Flierl (1986). In their study, the interaction of a point vortex with a jump discontinuity jet was considered on an f-plane. Their experiments illustrated a new eddy propagation tendency not associated with planetary rotation or background advection. If an anticyclonic eddy approaches normal to a jet, the negative vorticity of the eddy interacts with the cyclonic, positive vorticity side of the jet, and a weaker cyclonic eddy is formed. The propagation tendency of the eddy pair is determined by the addition of the two vorticities and the dipole is advected in the common direction.

This interaction of an eddy with a jet resulting in eddy motion was also demonstrated in Smith and Davis (1989), Figure 2.4, where eddies and jets with finite vorticity distributions were also considered. The extent to which these processes apply in a marginal ice zone situation is examined in this study.

In the previous eddy-jet interaction studies of Stern and Flierl (1986) and Smith and Davis (1989), the motion

of a vortex away from a jet was found for eddies initially within a nondimensional length scale, $R(o)$, from the edge of the jet. The nondimensional length scale depends on the vorticity of the eddy and its size. Smith and Davis (1989) found eddy motions for values of $R(o)$ in the range of .5 to 2.5, with insignificant eddy motion for greater $R(o)$. values. For comparison with Smith and Davis (1989), $R(o)$, in this study, is approximately 1.1 indicating that vortex motion induced by the jet is likely to occur.

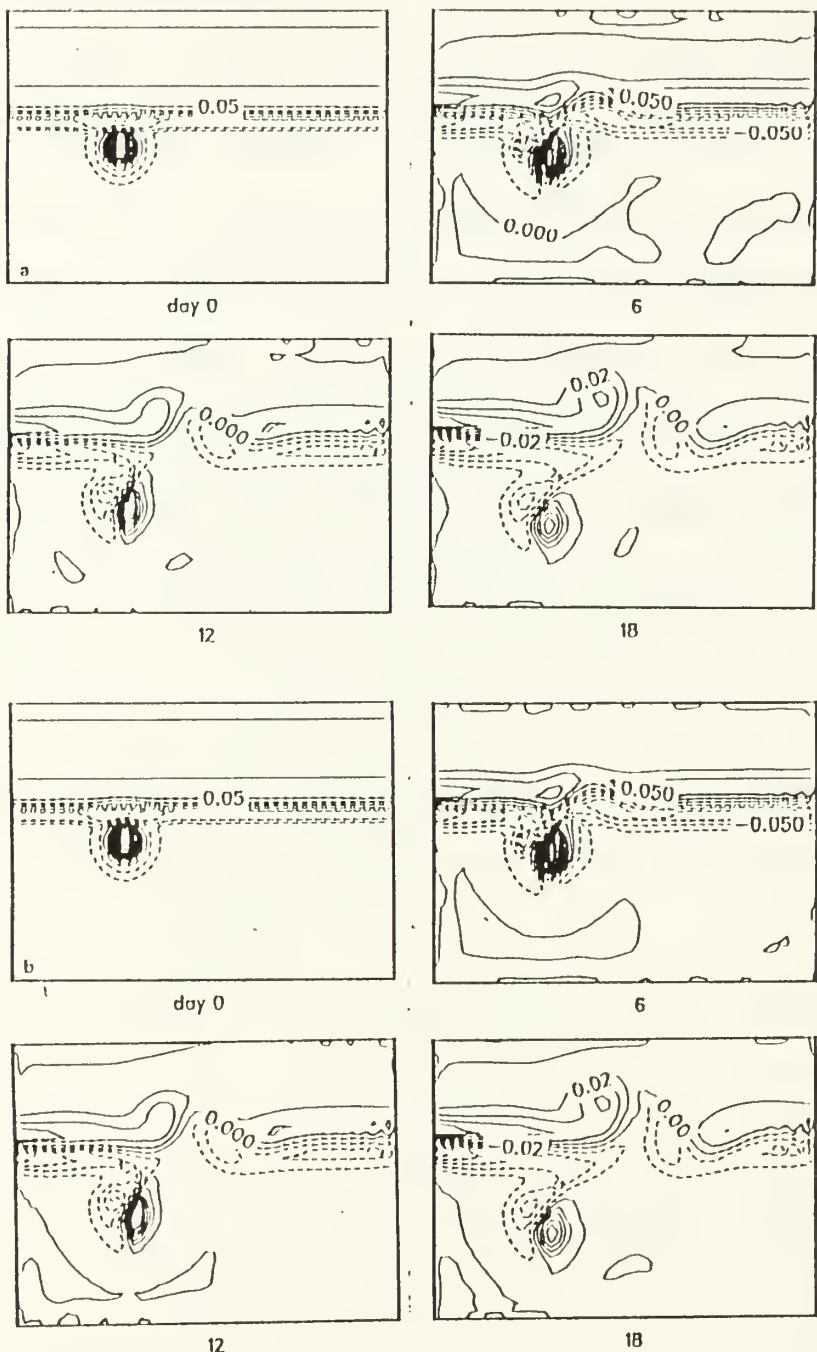


Figure 2.4 Eddy-Jet Interaction in the Absence of Ice (a) Upper Layer Relative Vorticity (b) Lower Layer Relative Vorticity (C.I. = $.05 \times 10^{-4} \text{ s}^{-1}$ for Day 0-6 and C.I. = $.02 \times 10^{-4} \text{ s}^{-1}$ for Day 12-18)

Source: Smith and Davis (1989)

D. ICEBANDING

Icebanding is a frequently observed dynamic phenomenon that occurs in the marginal ice zone. Icebanding is important because it causes a more rapid ablation of the ice margin according to Hakkinen (1986a). Hakkinen (1986a) examined several possible mechanisms for iceband formation and their typical size. First indications from satellite images are that the icebands are 10 km wide with approximately 10 km of ocean separating them. Later measurements taken by surface platforms indicate narrower icebands between .5 to 1 km. One of the theories cited by Hakkinen (1986a) is that internal waves cause icebanding. The wavelengths and phase speeds of internal waves in a two layer system are similar to the motion of the icebands. It is also suggested by Hakkinen (1986a) that previous studies demonstrate the formation of icebands by lee waves.

Hakkinen (1986a) also demonstrated the formation of icebands by modeling the ice edge with ice-ocean being coupled through interfacial stresses. The momentum flux used by Hakkinen (1986a) has an air-ice coupling three time greater than the air-ocean coupling. Along ice

(upwelling) winds were introduced that varied sinusoidally with a four day period. The along ice edge velocity would drive the cross ice edge Ekman flow and some icebanding would develop in 12 days. To have ice banding occur at least one wind reversal was necessary. This study illustrates similar results in a much shorter time by the introduction of an ocean jet along the ice edge.

III. NUMERICAL TECHNIQUE AND MODEL PARAMETERS

The numerical model was initialized with parameters chosen to resemble the East Greenland Current with a velocity of 30 cm/sec as observed by Gascard et al. (1988). A schematic of the model domain is presented in Figure 3.1. An ice edge in which concentration increased to the west was included and both cyclonic and anticyclonic eddies of 10 km diameter were examined in a time sequence. Foldvik et al. (1988) determined a typical tangential current speed in the observed eddies to be 15 cm/s. The initial eddy-jet interaction experiments are without winds. The effects of along ice upwelling and downwelling winds on the eddy-jet interaction are also considered. Topography simulating the continental slope off Greenland was also included in some runs to determine the effect on the eddy jet interaction. The determination of the various parameters will be discussed in chapter four.

A. THE OCEAN MODEL

The model used in this study is the same as that used by Smith et al. (1988) with the addition of a barotropic jet. Experiments are performed using a two-layer primitive equation semi-implicit numerical scheme. In most experiments the simulated ocean topography has a flat bottom. In several experiments the topography of the East Greenland Slope is represented by a linear bottom slope, sloping upward toward the west. The depth ranges from 4050 meters to 1050 meters at the boundary. The effects of topographic dispersion of the eddy are examined.

The model constants c_{ai} , c_{aw} , c_{lw} , etc. are chosen from Hakkinen (1986b) and are defined in the Appendix. The motion of each layer is governed by the momentum equation:

$$\frac{\partial \vec{V}_l}{\partial t} + (\nabla \cdot \vec{V}_l + \vec{V}_l \cdot \nabla) v_l + k \times f \vec{V}_l = - h_l \nabla P_l + A_h \nabla^2 \vec{V}_l + \frac{\delta_h}{\rho l} ((1 - A) \tau^{aw} + A \tau^{lw}) \quad (\text{eqn. 3.1})$$

and the continuity equation:

$$\frac{\partial h_l}{\partial t} + \nabla \cdot V_l = 0 \quad (\text{eqn. 3.2})$$

for layer ($i=1$ upper and $i=2$ lower) thickness h_i , and velocities v_i . The fluid is hydrostatic and Boussinesq. Fluid density (ρ_i) in each layer is fixed and no mixing across the fluid interface is allowed. The ocean-ice coupling is through the ice-water interfacial stress,

τ^{iw} :

$$\tau^{iw} = \rho_I c_{lw}(u_I - u_w) |u_I - u_w| \quad (\text{eqn. 3.3})$$

and concurrently, the ocean-air coupling through the air-water stress, τ^{aw} :

$$\tau^{aw} = \rho_a c_{aw}(u_a - u_w) |u_a - u_w| \quad (\text{eqn. 3.4})$$

for ice (u_I), air (u_a) and upper layer ocean (u_w) velocity vectors. The small-scale turbulent eddy dissipational processes are represented by a horizontal Laplacian operator on transport. The coefficient A_h has been chosen small ($10\text{m}^2\text{s}^{-1}$) making the fluid relatively inviscid, since the Laplacian operator only roughly represents a complex process. All notation is defined in appendix.

The semi-implicit scheme has been used in a number of mid-latitude ocean mesoscale circulation studies. A

thorough explanation by Hurlburt and Thompson (1980) and Smith and O'Brien (1983) provide more details of the scheme. They show how the model conserves mass and total energy in the absence of dissipation. The model verification of the Rossby dispersion characteristics was done by comparing linear analytic solutions to the linear test cases run on the model as discussed in Smith and Reid (1982). The characteristics of the upwelling and downwelling response at the ice edge are consistent with that seen in the models of Hakkinen (1986b), and Smedstad and Roed (1985).

B. BOUNDARY AND INITIAL CONDITIONS

A rectangular (111 x 79 km; i=111, j=79) finite difference gridded domain is used for the model. In order to align the domain with the East Greenland Current, it is rotated approximately 90 degrees relative to the referenced latitude of 80° N. This simulates a southward jet running approximately parallel to the east coast of Greenland. The initial state consists of a geostrophically balanced jet extending uniformly across the basin from north to south and a Gaussian eddy in gradient balance east of the jet. Experiments are

initialized with barotropic velocity distributions. While the East Greenland Current velocities at depth may be weaker than near the surface, this choice eliminates unstable meandering of the jet, simplifying the eddy-jet interaction. This also allows a more direct comparison with the previous eddy-jet study of Smith and Davis (1989).

The barotropic eddy and jet are defined in terms of upper (h_1) and lower (h_2) layer thickness.

$$h_1(v) = \bar{H}_1 \quad (\text{eqn 3.5})$$

and in the lower layer:

$$h_2(v) = \bar{H}_2 - A_j(1e \frac{-(y-y_0)^2}{2L_j^2}) (v \geq y_0) \quad \pm A_e(e \frac{-r^2}{2L_e^2}) \quad (\text{eqn. 3.6})$$

where a negative value is assigned for cyclones and a positive value for anticyclones. H_1 and H_2 are mean layer thickness values.

The eddy radius is defined as follows:

$$r^2 = (x - x_c)^2 + (y - y_c)^2 \quad (\text{eqn. 3.7})$$

The eddy center is located at the x_e , y_e coordinates. The eastern edge of the jet is at y_o (y grid point $j = 38$), 38 km from the eastern boundary. In this study the initial eddy location relative to the edge ($y=y_o$) of the jet, is fixed at ten km to the east. L_j and L_e are the e-folding width scales (= 5 km) for the jet and eddy. The amplitude of the Gaussian jet was chosen to give a maximum velocity (v_{max}) of approximately 30 cm/s in each layer in the base case experiments. This velocity is similar to observed velocities of the East Greenland Current (Gascard et al. 1988). A radiation condition was used on the downstream (left) boundary in all model simulations. The radiation condition, (Camerlengo and O'Brien 1980), advects flow out of the basin at speed $\frac{\Delta x}{\Delta t}$, when flow is outward adjacent to the boundary. On the upstream boundary (right), constant jet inflow of the form of the initial condition is continually maintained. The north and south boundaries are no-slip walls where both tangential and normal flow are set equal to zero. The initial condition parameters are provided in the appendix. The thermocline depth in the East Greenland Current ranges from 25-100 meters. The upper layer mean thickness was chosen to be 50 meters in

all cases. The lower layer mean thickness is 4000 meters. This gives a first internal Rossby radius of deformation (R_d) equal to 5 to 7 km, consistent with the observations of Johannessen et al. (1983). Nondimensional eddy size $\gamma = \frac{L}{R_d}$ is thus order 1. The Rossby number for this flow ($\frac{v_{max}}{fL}$) is .21 so the nonlinear terms can not be neglected in the momentum equations.

In the wind driven simulations, spatially uniform winds are specified (10m/s) along the ice edge. As in previous studies, Hakkinen (1986b), Smith et al. (1988), the wind vector has been rotated to offset cross ice edge drift associated with the ocean Ekman drift to the right. The angle of rotation which gave the minimal meridional ice edge drift was found to be 25° to the left of ice edge orientation. The simulations are integrated for duration of 6.5 days, within which significant eddy jet interactions occur. The eddies and jet are initialized with barotropic structure but baroclinic structure in the interface is free to develop during the model run.

C. THE ICE MODEL

The ice model is initialized so the ice edge runs parallel to the jet. The motion of the ice is governed by the momentum equations (eqn. 3.8 and 3.9) and the continuity equations (eqn. 3.10 and 3.11). Although the ice is initially at rest, adjustments to an equilibrium state occurs rapidly, normally one-half day.

$$\frac{\partial u_I}{\partial t} + u_I \frac{\partial u_I}{\partial x} + v_I \frac{\partial u_I}{\partial y} = f v_I + \frac{A}{m} (\tau_x^{ai} - \tau_x^{iw}) - g \frac{\partial(h_1 + h_2)}{\partial x} \quad (\text{eqn. 3.8})$$

$$\frac{\partial v_I}{\partial t} + u_I \frac{\partial v_I}{\partial x} + v_I \frac{\partial v_I}{\partial y} = -f u_I + \frac{A}{m} (\tau_y^{ai} - \tau_y^{iw}) - g \frac{\partial(h_1 + h_2)}{\partial y} \quad (\text{eqn. 3.9})$$

$$\frac{\partial m}{\partial t} + \frac{\partial(mu_I)}{\partial x} + \frac{\partial(mv_I)}{\partial y} = A_m \nabla^2 m \quad (\text{eqn. 3.10})$$

$$\frac{\partial A}{\partial t} + \frac{\partial(Au_I)}{\partial x} + \frac{\partial(Av_I)}{\partial y} = A_a \nabla^2 A \quad (\text{eqn. 3.11})$$

The ice concentration is represented by (A) and the ice mass per unit area by (m). The air-ice coupling for the x component is represented using equation 3.12 and for the y component using equation 3.13.

$$\tau_x^{ai} = \rho_a C_{ai} (u_a - u_I) |u_a - u_I| \quad (\text{eqn. 3.12})$$

$$\tau_y^{ai} = \rho_a C_{ai} (v_a - v_I) |v_a - v_I| \quad (\text{eqn. 3.13})$$

Ice thickness (D) is computed using equation 3.14, with an initial thickness of 2 meters. The concentration is initialized at 05% at the open ocean boundary and 75% at the western boundary, Figure 3.2.

$$D = \frac{m}{(\rho_I A)} \quad (\text{eqn. 3.14})$$

Most mesoscale studies neglect the pressure gradient force in ice associated with the sea surface slope, but Smith et al. (1988) showed that it should be included in the ice equations in no wind or light wind studies. The Laplacian damping term has also been included in the continuity equation (eqn. 3.10), as in previous studies such as Hakkinen (1986b) and Hibler (1979). Since dynamic effects are the focus of this study, no internal stress terms are considered, an assumption which is appropriate for ice concentrations less than 85% (Hibler 1979, 1984).

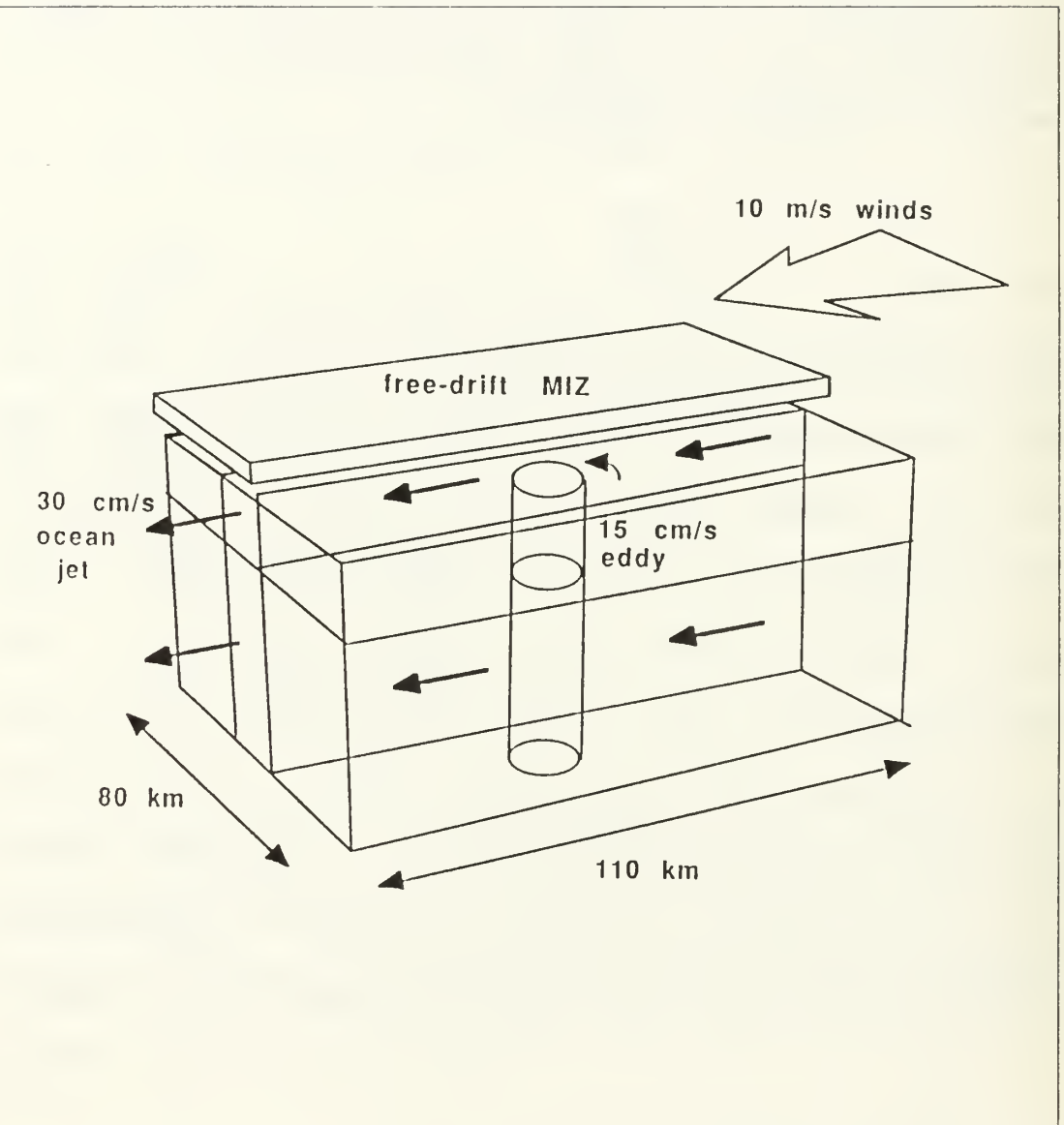


Figure 3.1 Coupled Ice Model and Initial Conditions

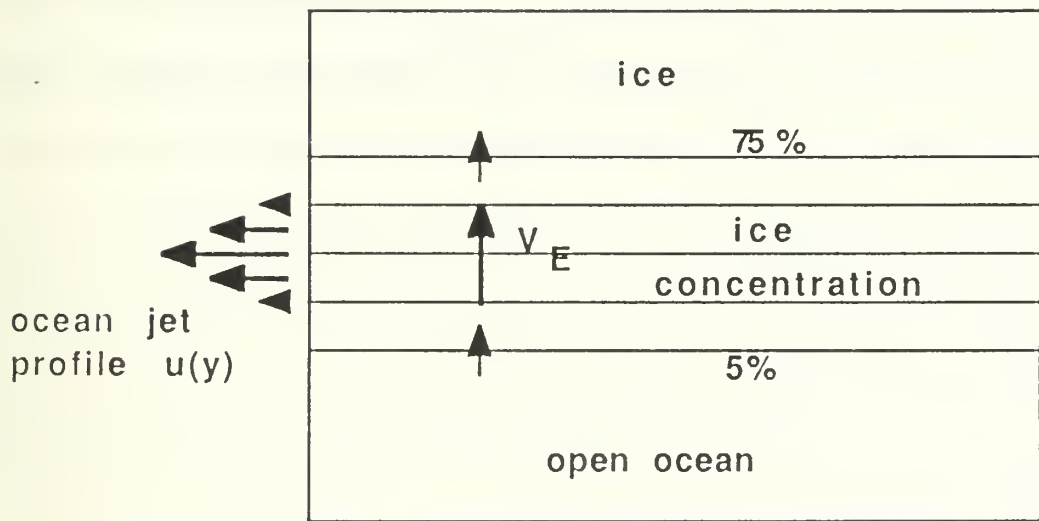


Figure 3.2 Ekman Divergence in Ice Concentration Over a Laterally Sheared Ocean Jet

D. WIND FORCING

In some experiments wind forcing is included to determine the effect on the eddy-jet interaction. The winds are either upwelling favorable (ice edge to the right) or downwelling favorable (ice edge to the left). The predominant wind direction is seasonally dependent but during MIZEX-84, Johannessen (1987) observed predominantly northerly and southerly flow, Figure 4.1.

IV. EXPERIMENTS

A. PURPOSE OF EXPERIMENTS

The purpose of the following experiments is to understand the effect of eddy-jet interactions along an ice edge. Observed dynamic features such as upwelling/downwelling, dipole formation, icebanding, and ice transport (ice tongues) will be examined using the numerical model. The output of the numerical model runs produced a time sequence, .5 day interval, of the ice concentration, upper level relative vorticity, lower level relative vorticity, surface height anomaly and the interface height anomaly.

B. PRELIMINARY EXPERIMENTS

A list of primary parameters is provided in the appendix. Table 1 gives a summary of the parameters varied during each experiment.

Before examining the eddy-jet interaction in the MIZ a base case experiment is conducted to examine the effects of a jet running parallel to and under the ice edge. The

eddy was not included in the model initial conditions for this run.

1. Simulations with No Wind

a. *Experiment 1A* (Jet/Ice edge simulation)

In this simulation a 30 cm/s jet was initialized under and parallel to an ice edge without winds. The experiment is limited to a duration of 6.5 days by computing constraints, however this is sufficient to examine the eddy-jet interaction processes of this study. It is important to note that icebanding has only been simulated in numerical modeling by a time reversing wind, Hakkinen (1986a) or upwelling favorable winds , (30° off ice edge with ice to the right) Smedstad and Roed (1985). This simulation illustrates that iceband formation can occur without winds.

A time sequence of the ice concentration field for the base case, day 1, 2, and 4 is shown in Figure 4.2. By day four a decrease in ice concentration above the jet can be observed. In order to quantify these data a cross section normal to the ice at midbasin of ocean \mathbf{u} velocity and ice concentration was taken for each day. On day 1, the ice concentration over the jet shows a decrease from .75 to

.60 over a 5 km band in the domain, (Figure 4.3). The minimum ice concentration is located over the maximum \mathbf{u} velocity of 30 cm/s. On day 2 (Figure 4.4), the ice concentration over the jet shows a decrease in ice concentration from greater than .80 to .40 and then back to .80 over the 10 km maximum \mathbf{u} velocity area. This 50% decrease shows substantial banding beginning to occur in just two days. By day 4, (Figure 4.5), the ice concentration shows a decrease from greater than .80 to less than .40 over the \mathbf{u} maximum velocity 10 km area. It is also evident that the ice band is beginning to move slightly westward of the jet.

Since there is no wind in this simulation, the cause of the ice banding is the ocean induced Ekman transport in the ice. Since the \mathbf{u} maximum of a laterally sheared jet has a maximum Ekman transport (to the right in the northern hemisphere), a divergence occurs over this maximum, Figure 3.2. This effect tends to transport ice normal to the \mathbf{u} velocity maximum creating an iceband to the left. The formation of an iceband is a function of the ocean \mathbf{u} velocity and the larger the ocean \mathbf{u} velocity maximum, the greater the ice \mathbf{v} component or Ekman

transport. It appears that by day 4 the entire iceband is beginning to drift with the Ekman transport across the domain.

Although Smedstad and Roed (1985) were able to simulate an iceband by upwelling favorable winds in 12 days, this study is different in that the numerical model includes a surface tilt term in the momentum equations to balance the Coriolis term. The inclusion of the surface tilt term results in a smaller iceband than that seen in Smedstad and Roed (1985). In Smedstad and Roed (1985), the along ice edge upwelling favorable winds create the jet which then causes divergence in the ice. In this study, the jet simulating the East Greenland Current, in the absence of winds, causes the divergence.

Another interesting result is that for a jet of 15 cm/s or less the icebanding did not develop in 6.5 days. The jet has to be stronger than 15 cm/s to create sufficient transport to cause a divergence in the ice during this period.

2. Simulation with Wind

Smith et al. (1988) conducted a study of the effect of upwelling winds on ocean eddies along an ice edge but

did not consider the effect of a jet running parallel to the ice edge.

a. Experiment 1B (Jet ice edge simulation with upwelling favorable winds)

The initial conditions in this simulation are the same as in the previous run; however upwelling favorable winds are added. Based on the findings of Smedstad and Roed (1985), it was expected that the upwelling winds would supplement the icebanding by augmenting the upwelling and thus the iceband. A cross section of ice concentration and \mathbf{u} velocity, Figure 4.6 indicates that this is not the case. The concentration decreases less than 10% on day 4. The upwelling band is present at the interface by day 6, Figure 4.7, but the iceband is not as pronounced in the jet only case. This is consistent with the findings of Smith et al. (1988). Along ice edge 10 m/s winds contribute more to the ice momentum balance than does the ocean. Thus while the ocean jet causes some divergence in the ice, the dominant velocity is wind driven to the south. Computational considerations stopped the model at day 6 so a longer run time may have shown the iceband occurring as in Smedstad and Roed (1985). The important inference is that a jet,

such as the East Greenland Current may create an iceband on time scales as short as one day, thus contributing to a more rapid ablation of the ice edge.

TABLE 1. SUMMARY OF EXPERIMENTS

EXP #	JET	EDDY (15cm/s)	WIND DIRECTION	WIND SPEED	TOPOGRAPHY
1A	30 cm/s	none	none	none	flat
1B	30 cm/s	none	upwelling favorable	10 m/s	flat
2A	30 cm/s	A/C	none	none	flat
2B	30 cm/s	CYC.	none	none	flat
3A	30 cm/s	A/C	upwelling favorable	10 m/s	flat
3B	30 cm/s	A/C	downwelling favorable	10 m/s	flat
4A	30 cm/s	CYC.	upwelling favorable	10 m/s	flat
4B	30 cm/s	CYC.	downwelling favorable	10 m/s	flat

upwelling favorable is 205° relative to north
 downwelling favorable is 025° relative to north

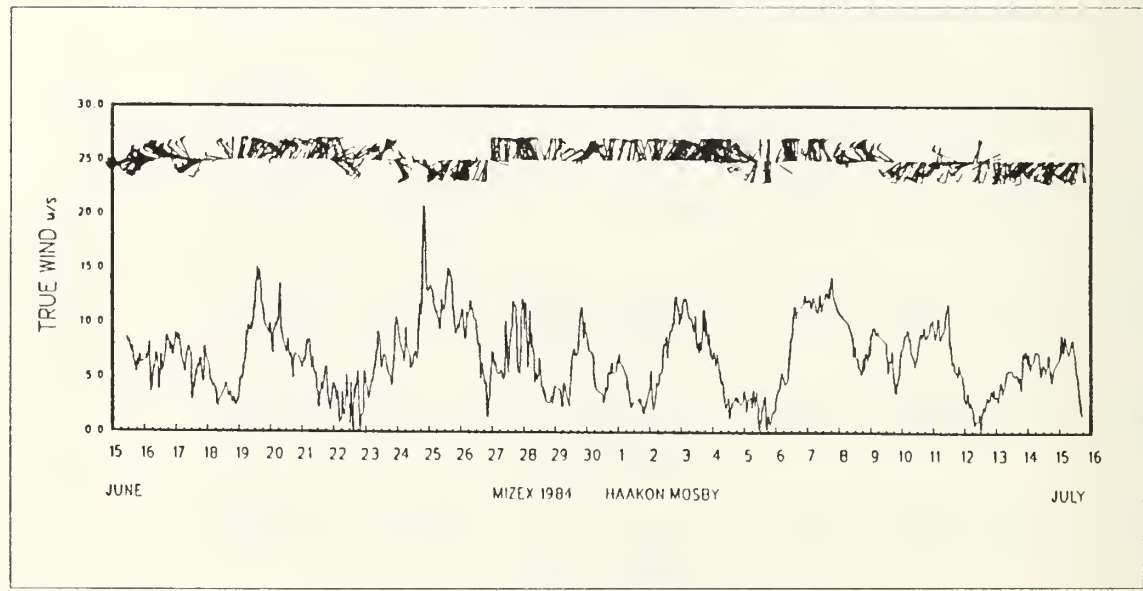
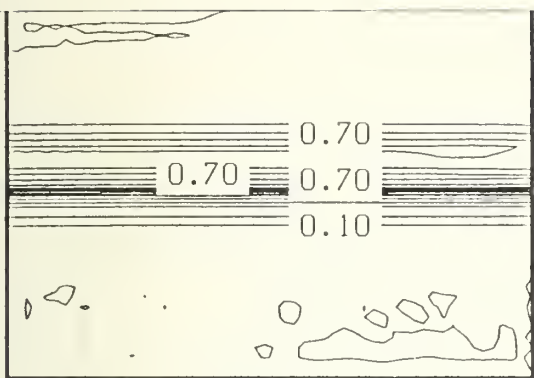
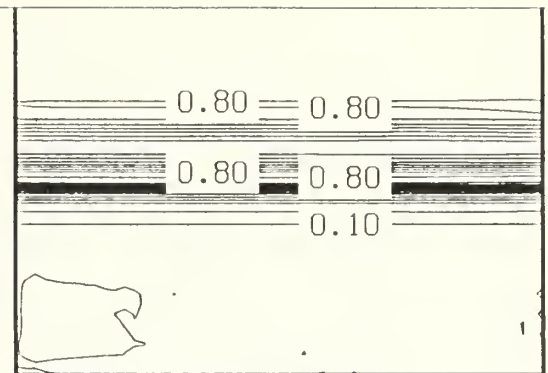


Figure 4.1 Fram Strait, Mean Wind Direction and Speed
(30 minute averages)

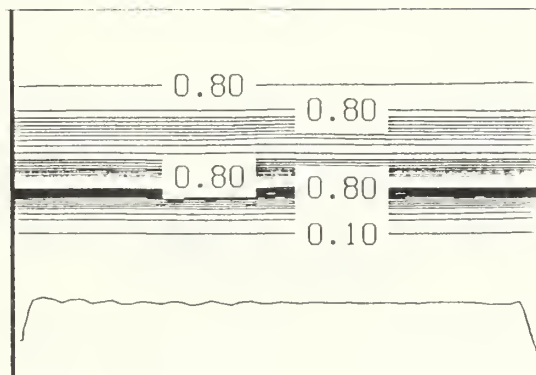
Source: Johannessen et al. (1987)



DAY 1



DAY 2



DAY 4

Figure 4.2 Ice Concentration Days 1, 2, and 4
 (Jet-Ice Edge with No Wind, Experiment 1A)
 Contour Interval .05
 (Dimensions in this and subsequent domain
 contour plots are 79 x 111 km)

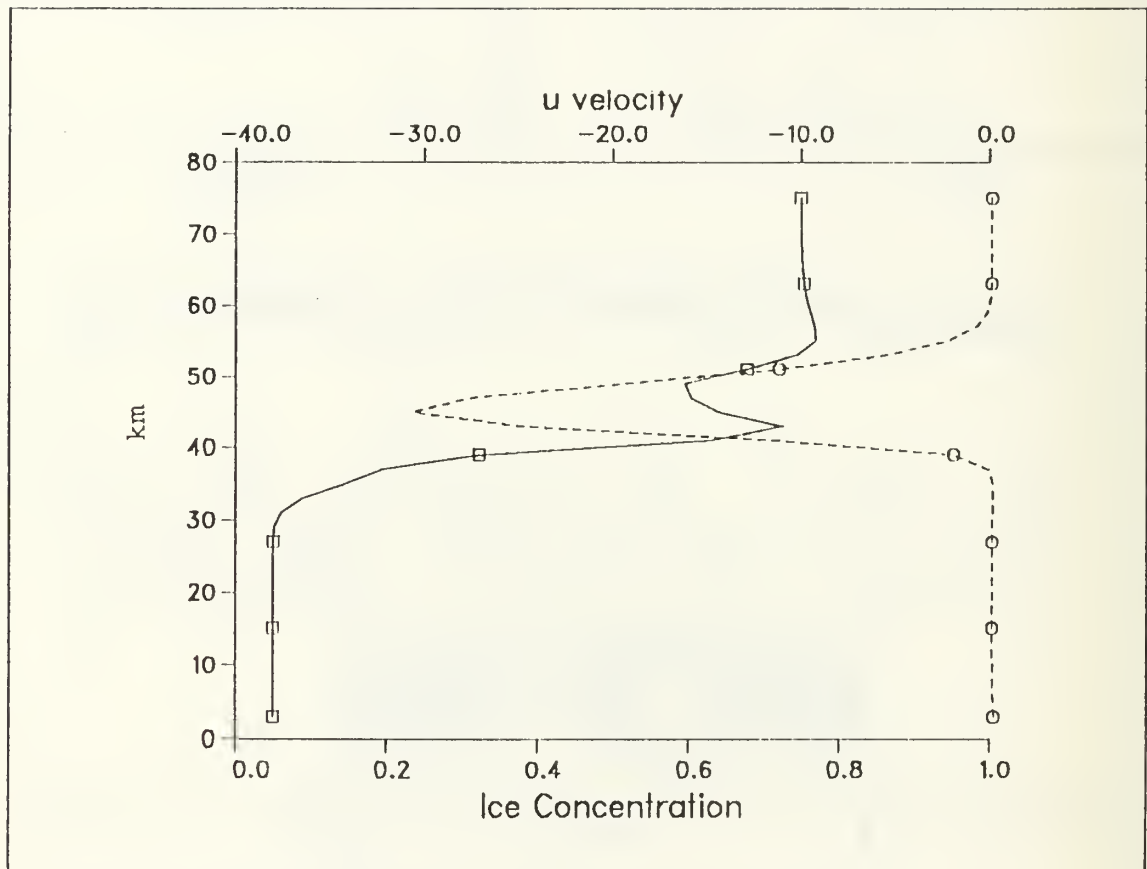


Figure 4.3 **u** Velocity and Ice Concentration Across MIZ, Day 1 (Solid line - ice concentration and dashed line - **u** velocity)
 (Jet-Ice Edge with No Wind, Experiment 1A)

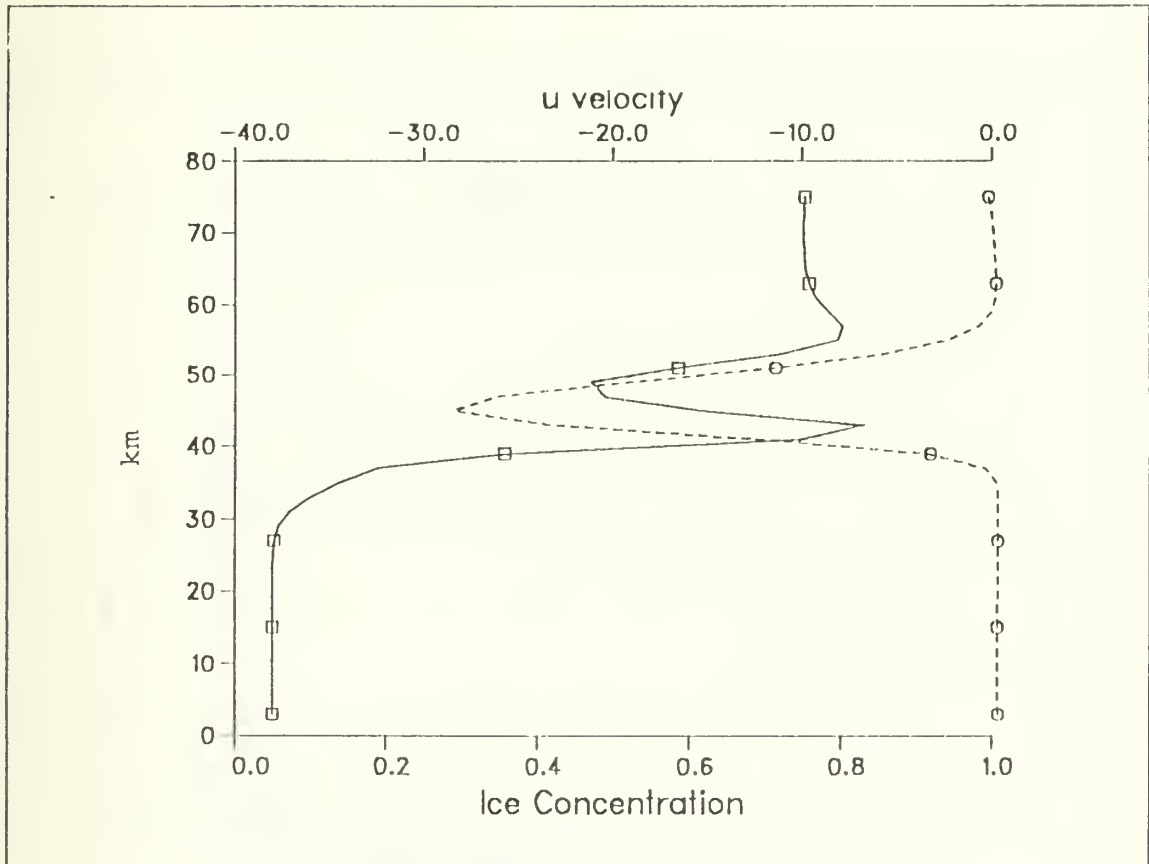


Figure 4.4 \mathbf{u} Velocity and Ice Concentration Across MIZ,
Day 2 (Solid line - ice concentration and
dashed line - \mathbf{u} velocity)
(Jet-Ice Edge with no wind Experiment 1A)

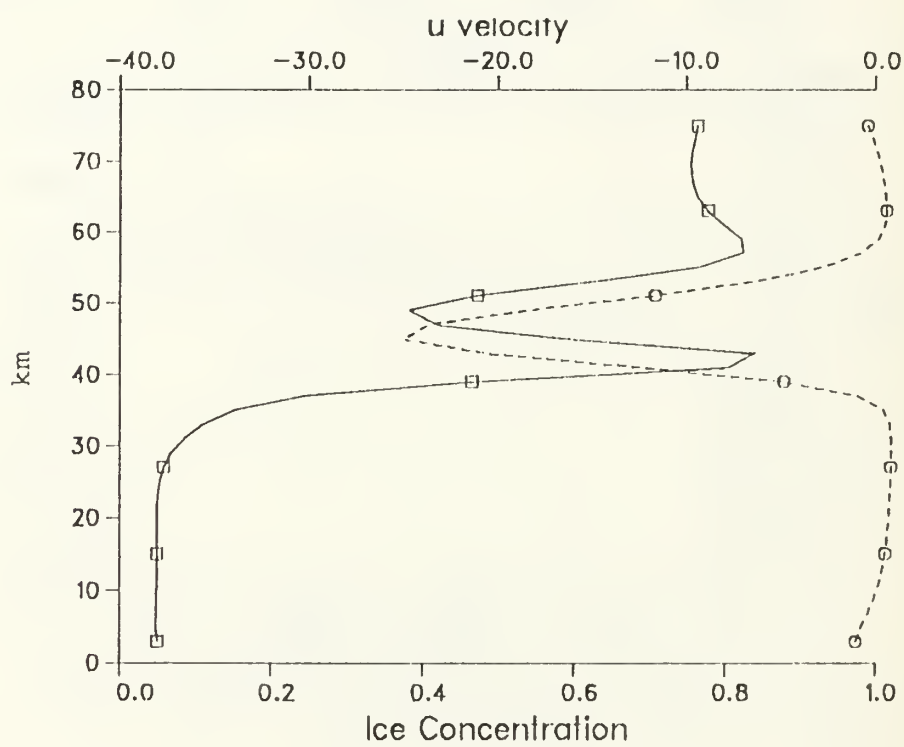


Figure 4.5 **u** Velocity and Ice Concentration Across MIZ, Day 4 (Solid line - ice concentration and dashed line - **u** velocity)
 (Jet-Ice Edge with no wind Experiment 1A)

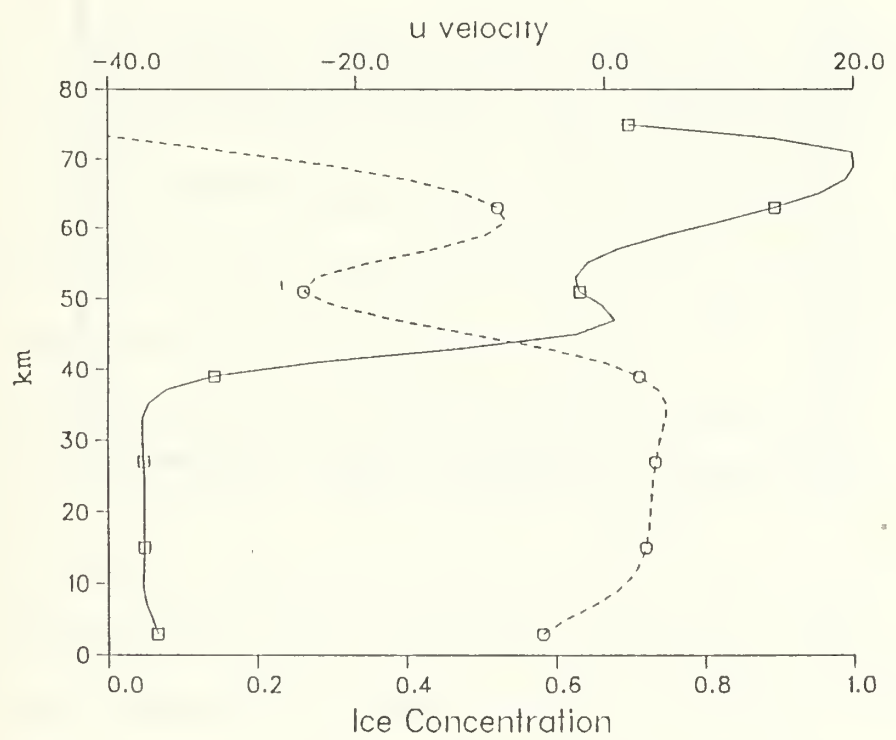
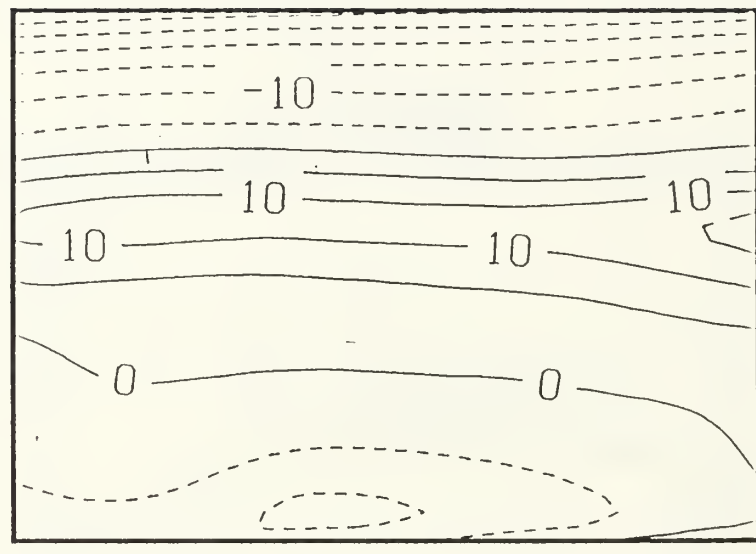


Figure 4.6 **u** Velocity and Ice Concentration Across MIZ, Day 4 (Solid line - ice concentration and dashed line - **u** velocity)
 (Jet-Ice Edge with upwelling winds, Experiment 1B)



6.0

Figure 4.7 Interfacial Height Anomaly (meters) Day 6
(Jet-Ice Edge with Upwelling Winds,
Experiment 1B)

C. PRIMARY EXPERIMENTS

1. Experiment 2A (Base Case: Anticyclone-Jet no wind)

The anticyclone/jet interaction in the marginal ice zone was chosen as the base case to demonstrate the production of a dipole from a monopole vortex. The experiment begins with the anticyclone adjacent to the cyclonic (and seaward) side of the laterally sheared jet (see Figure 4.8, day 0). It has been shown by Smith and Davis (1989) that when an eddy interacts with a stable barotropic zonal jet, vortex pairing occurs and the eddy propagates away from the jet. Figure 4.8 demonstrates that this process can occur for East Greenland Current parameters as well. As is seen in the upper layer vorticity field, the anticyclonic vorticity from the eddy is interacting with the cyclonic vorticity side of the jet. This interaction causes a small cyclonic vortex to separate from the jet. The dipole persists through day 6 propagating away from the ice edge. This propagation is consistent with the interaction of opposite vorticities which contribute to a common propagation direction.

The movement of the ice edge in response to the interaction is shown in Figure 4.9. The first indication

of an interaction is the perturbation created on day 1. The newly formed cyclonic vortex is advecting ice out away from the ice edge creating an ice tongue. Observations of the ice tongues are not uncommon (Gascard 1988). As the experiment continues to day 6, the ice tongue extends seaward approximately 10 km and is centered primarily over the cyclonic vortex. This could be one of the reasons mostly cyclonic ice swirl eddies are observed in imagery. The Synthetic Aperture Radar Imagery from MIZEX 1987, Figure 4.10, shows the advection of ice off the ice edge is a manner consistent with eddy-jet dipole formation.

Another interesting phenomena from this base case is the sinuous ice edge that occurs from the initial eddy-jet interaction. Hakkinen (1986b) showed that if the model was initialized with a sinuous ice edge, differential Ekman pumping would spin up anticyclonic and cyclonic eddies in the upper ocean. This study shows that another mechanism can cause a sinuous ice edge is an eddy-jet interaction. The initial perturbation in the jet is advected downstream with the mean flow and another dipole occurs from this interaction. Figure 4.8 demonstrates how the perturbation in the cyclonic side of the jet causes a

cyclonic vortex to spin up downstream which interacts with the anticyclonic side of the jet causing an anticyclonic vortex to spin up adjacent to it. The ice concentration as seen in Figure 4.9 is highly variable downstream creating a complicated ice edge and open areas in the interior ice pack within six days. Ice perturbations downstream of eddy-jet interactions are also documented in the observations of Gascard et al. (1988).

Gascard et al. (1988) observed that the initial perturbation caused by a cyclonic eddy interaction with the East Greenland Current produces two intermediate cyclones downstream with a separation distance of 90 km. Since the period of an eddy is two to three days and the East Greenland current has a velocity of 30 cm/s, 90 km is approximately the distance a parcel will travel in that period of time. Gascard et al. (1988) also discussed eddies with a wavelength of 50 km, one-half of the previous wavelength. This is attributed to eddies developing a two ice tongue system with one ice tongue to the north and one to the south. The southern ice tongue is related to the off ice entrainment due to the cyclonic rotation and the northern ice tongue from a divergence

area upstream. The wavelength of the perturbations observed in this study is approximately 90 km and the downstream perturbations are observed for both cyclone and anticyclone-jet interactions.

2. Experiment 2B (Cyclone-Jet without winds)

Twelve of the fourteen eddies observed by Johannessen et al. (1987) in the MIZEX 84 data were cyclonic. Thus the only parameter in this experiment differing from experiment 2A is the sign of the eddy rotation. The results, however are markedly different. Figure 4.11 shows the vorticity distributions in the upper layer. On day 1 the cyclone has just started to perturb the jet. By day 4 the jet is slightly sinuous and by day 6, the initial perturbation is advected to the downstream boundary.

Figure 4.12 shows the effect of the cyclone-jet interaction on the ice concentration. On days 1 and 2 there is a weak ice tongue being advected cyclonically away from the ice edge. By day 3 the jet appears to advect the ice tongue downstream and smooths it out. On days 4, 5, and 6 the ice tongue is gone and only the perturbation from the cyclone can be seen. The reason ice

is not advected away from the ice edge as in experiment 2A is because the cyclonic eddy is interacting with the cyclonic side of the jet. Since both vorticities are of the same sign, no dipole is formed and no propagation mechanism exists to advect ice away from the ice edge. The eddies in experiment 2A or 2B do not have any effect on the icebanding; the iceband forms as it did in the preliminary experiments but tends to conform to the sinuous pattern caused by the eddy interaction.

3. Experiment 3A (Anticyclone/Jet with Upwelling Winds)

This experiment will examine the effect of upwelling winds on the anticyclone-jet interaction. Figure 4.13 shows the dramatic effect of the wind on the upper level vorticity. In the anticyclone-jet with no winds, experiment 2A, the dipole developed rapidly, but in this experiment with upwelling winds the process seems to be damped by the winds. It is observed that a weak dipole develops but by day 4 the anticyclone has become very weak. Figure 4.14 shows the lower level vorticity pattern and the characteristic dipole observed in experiment 2A is readily evident. Figures 4.15A and 4.15B contrast the velocity vectors in the no wind experiment 2A

with this experiment which has upwelling winds. In the upwelling wind case, an upwelling band develops on the eastern boundary due to boundary conditions. This creates a 10-15 cm/s jet opposing the anticyclone, thus damping the anticyclone in comparison to the no wind case. Figure 4.16 shows the effect of the interaction on the ice edge. The initial perturbation is advected downstream and by day six the ice edge is relatively smooth. An iceband comparable to the jet-only upwelling wind case, Experiment 1B is seen in this experiment as well.

Figure 4.17 characterizes the interface height anomaly between the two layers and by day 6, the interface has upwelled 10 meters height in the middle of the domain. As in previous studies, along ice edge winds with ice to the right cause this upwelling. It is also apparent in the figure that the upwelled interface is steeper under the higher concentration ice. Hakkinen (1986b) showed that when pycnocline changes are similar to upper layer thickness, non-linear effects can be important. In the case of upwelling winds, the Ekman driven flow advects the upwelling band iceward providing asymmetry. This is illustrated in Figure 4.18 by examining distance vs. time

($x-t$). At day 5, there is a gradual slope up to the 14 meter pycnocline anomaly then a sharp drop as the ice edge is neared at $x = 100$. It is readily apparent that the slope is gradual up to the 10 meter interface height anomaly and steep on the ice edge side of the upwelling band. This phenomenon has also been observed in the East Greenland Current marginal ice zone by Johannessen et al. (1983). Hakkinen (1986a) also stated that the wind forced jet caused the ice to move faster at the ice edge than it moved inside the ice pack.

In this experiment ice is not advected away from the ice edge in the presence of upwelling winds because a wind, greater than or equal to 10 m/s will dominate the ice dynamics. The cyclonic vorticity at the ice edge, induced by upwelling favorable winds, adds to the cyclonic vorticity of the jet and subtracts from the anticyclonic vorticity of the jet, Figure 4.19. The anticyclone is initially at $j=30$ to the south of this wind induced cyclonic vorticity. Its decay thus appears unrelated to the wind. The eastern boundary develops an upwelling band with a jet opposing the anticyclone. The anticyclone is damped by the artificial jet before a strong dipole can

form. The initial ice perturbation is advected downstream with the mean flow. The upwelling wind makes the ice edge less sinuous.

4. Experiment 3B (Anticyclone/Jet with Downwelling winds)

An anticyclone-jet experiment is conducted to see the effects of a downwelling favorable winds, (ice edge to the left), on the eddy-jet interaction. Since the winds are opposing the jet, the jet is substantially damped in the upper layer as evidenced by the decreasing gradient in the surface height anomaly, Figure 4.20. The winds provide anticyclonic vorticity to the jet, damping the cyclonic shear needed for dipole formation. There is no dipole formation and the characteristic ice edge of experiment 2A on day 2 contrasts vastly with the ice edge on day 2 of this experiment. Once again the wind forcing dominates the ice dynamics of the experiment.

5. Experiment 4A (Cyclone-Jet Interaction with Upwelling favorable winds)

This experiment demonstrates that upwelling favorable winds damp the cyclone-jet interaction in the upper level but generate a downstream cyclonic eddy due to differential Ekman pumping. This experiment is first

conducted using a velocity of 30 cm/s for both the eddy and the jet. The stronger eddy causes a stronger perturbation in the ice edge hence making the ice edge more sinuous, Figure 4.21. The upwelling band is interrupted by a downwelling band in the sinuous ice edge, Figure 2.2, appearing to spin up a downstream cyclone with a 15 meter amplitude seen in the interface, (Figure 4.22). Whereas experiment 2B, cyclone-jet interaction with no wind, shows a sinuous ice edge and upper level cyclonic vorticity out to day six, this experiment shows the upper level cyclonic vorticity weakening by day five, Figure 4.23. The cyclonic vorticity is however stronger than the corresponding upwelling wind anticyclone case. The ice edge is less sinuous than the no wind case and the initial perturbation is advected downstream with the mean flow of the jet. This case was run again with an eddy with a rotational velocity of 15 cm/s and a jet of 30 cm/s. Similar dynamics are observed; however, the stronger eddy creates the stronger perturbation which enhances the downstream eddy formation.

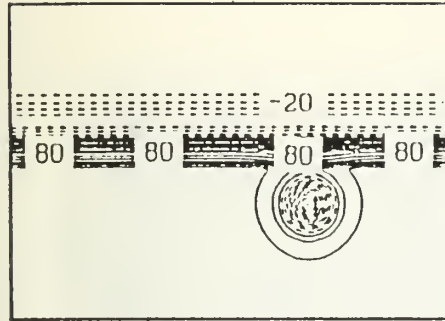
An important aspect of this simulation is that the winds blowing along the sinuous ice edge create a

downstream cyclonic eddy as evidenced by the 15 meter interface height anomaly. The generation of this downstream cyclonic eddy is consistent with the generation theory of Hakkinen (1986b). The eddy-jet interaction provides the mechanism for the sinuous ice edge assumed in the Hakkinen (1986a) study. Another interesting aspect of this mechanism for ice distortion is that unstable meandering of the jet is not required.

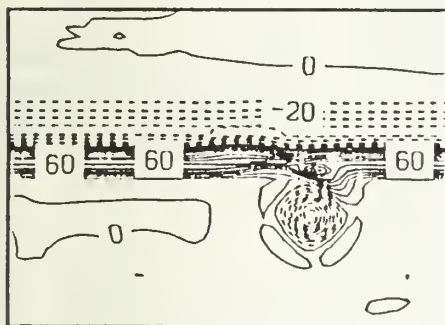
6. Experiment 4B (Cyclone-Jet with Downwelling winds)

This experiment is conducted to contrast with experiment 3B and experiment 4A. The cyclone-jet with downwelling winds did cause the formation of a small ice tongue during the initial interaction in contrast to the anticyclone-jet with downwelling winds (Figure 4.24).

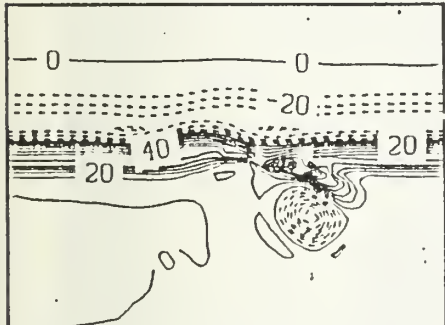
The primary difference between this and experiment 4A is that the downwelling winds oppose the jet and inhibit the advection of the ice tongue downstream with the mean flow. The ice tongue remains stationary through day two. The downwelling band of five meters in the interface height anomaly supports the expected results from the downwelling favorable winds discussed by Hakkinen (1986b).



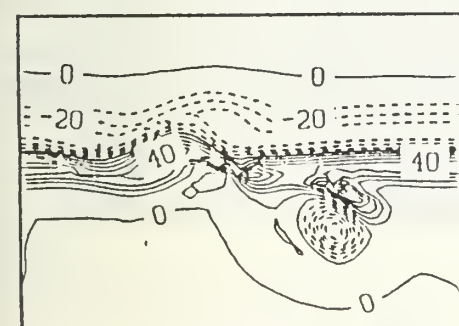
DAY 0



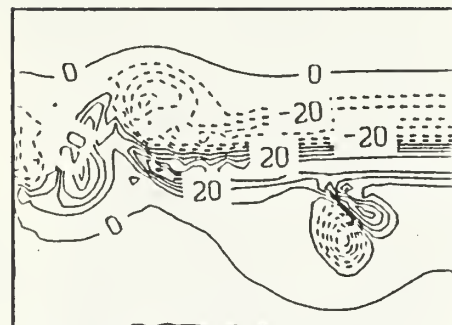
DAY 1



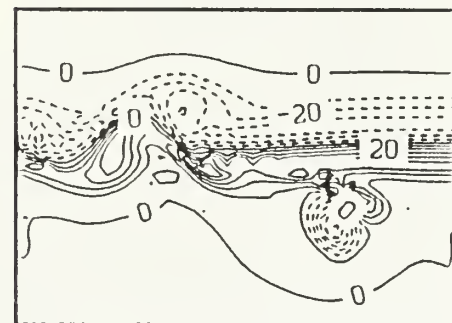
DAY 2



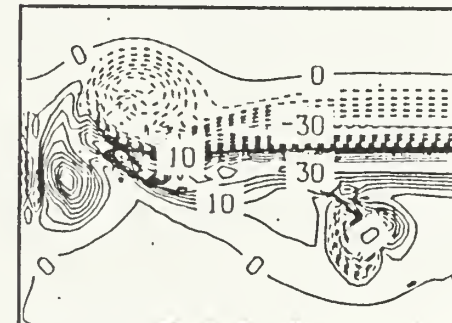
DAY 3



DAY 4

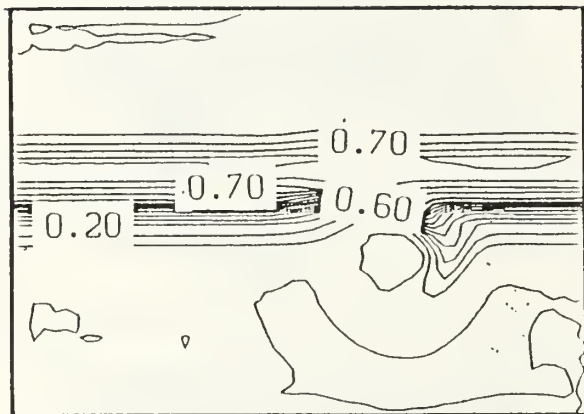


DAY 5

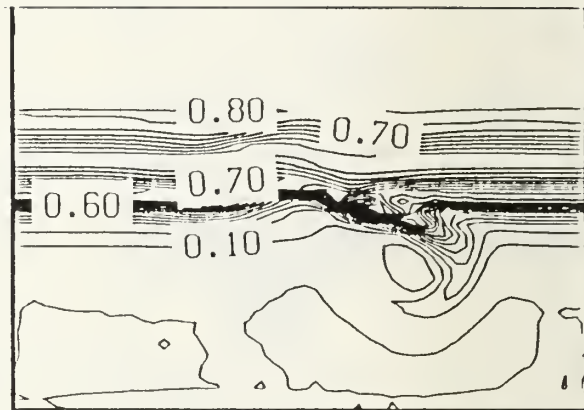


DAY 6

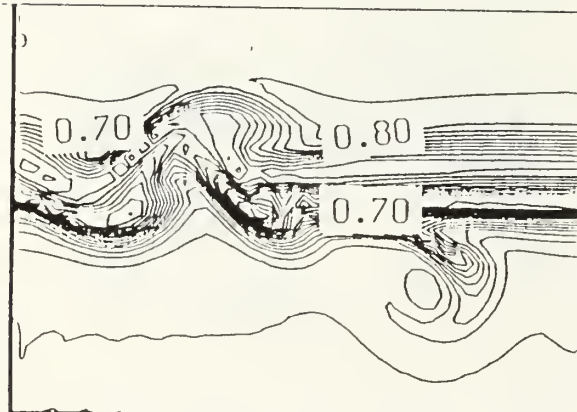
Figure 4.8 Upper Level Relative Vorticity ($\ast 10^{-6}$) Day 0-6 (Anticyclone-jet with no wind, Experiment 2A)



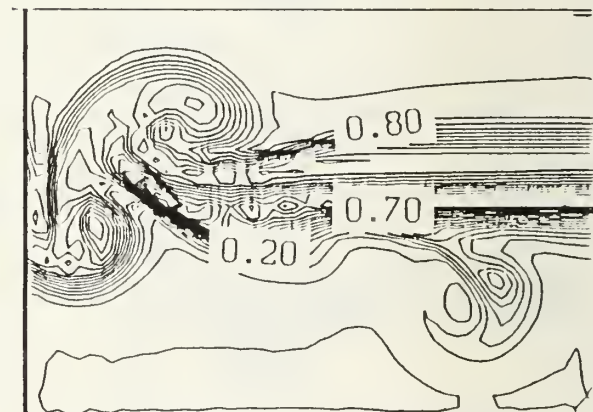
DAY 1



DAY 2

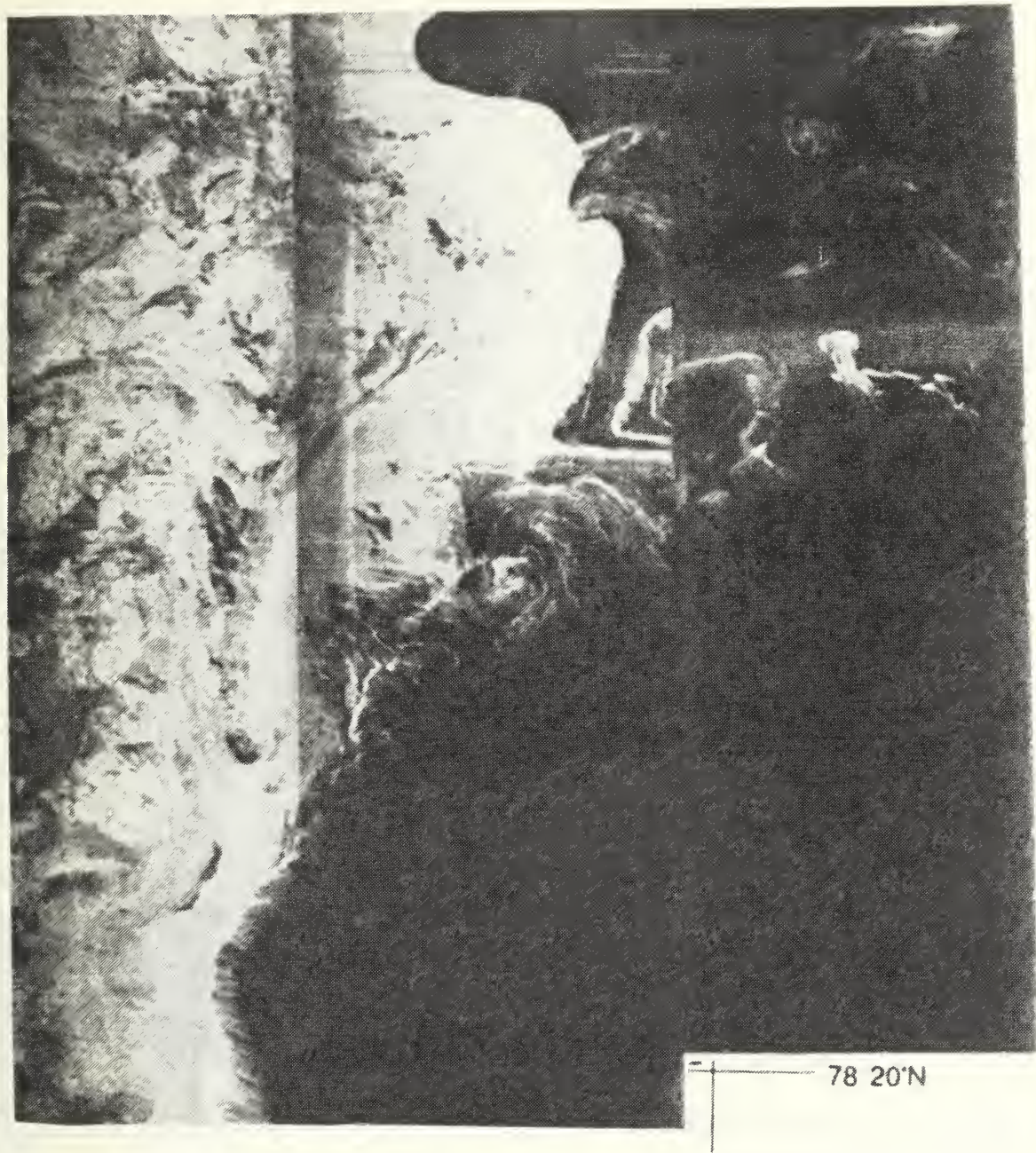


DAY 4



DAY 6

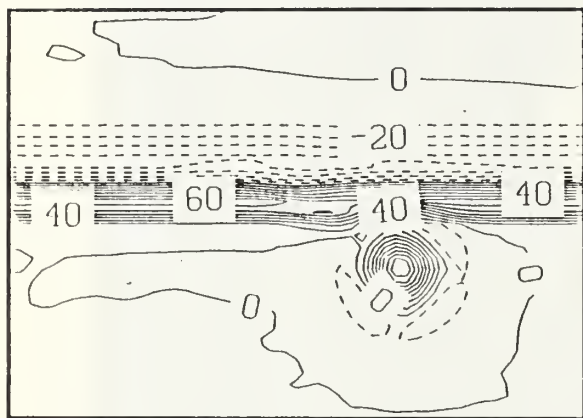
Figure 4.9 Ice Concentration for Day 1, 2, 4, and 6
(Anticyclone-jet with no wind, Experiment 2A (Contour interval .05))



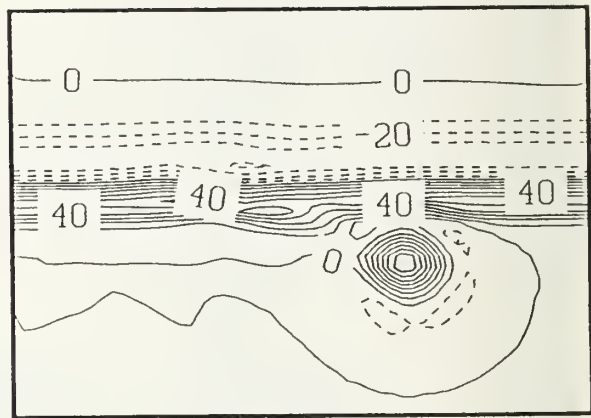
Light area to left is ice edge
Dark area to right is open ocean
(Possible dipole in center of domain)

Figure 4.10 Synthetic Aperture Radar Imagery MIZEX 1987

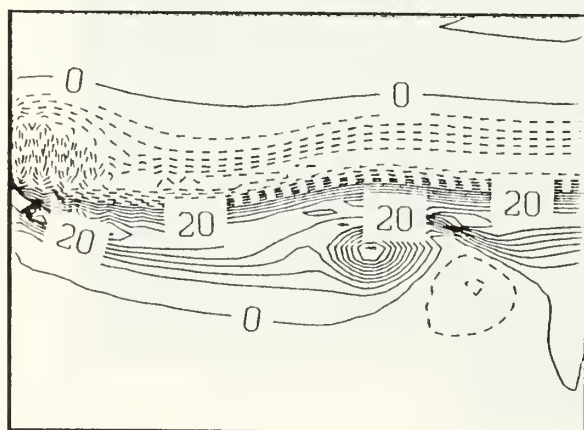
Source: Shuchman (1988)



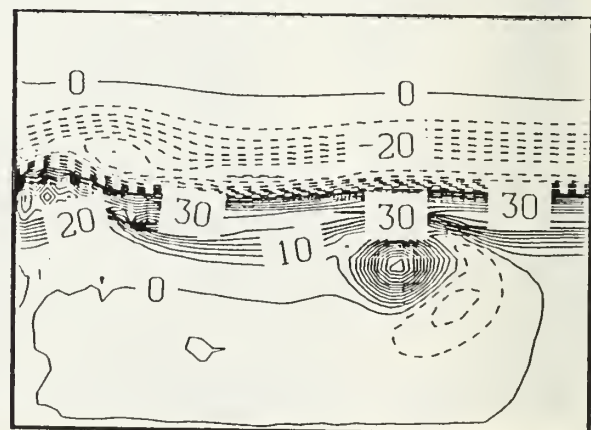
DAY 1



DAY 2

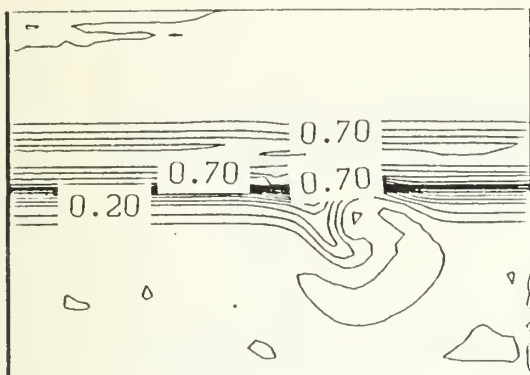


DAY 4

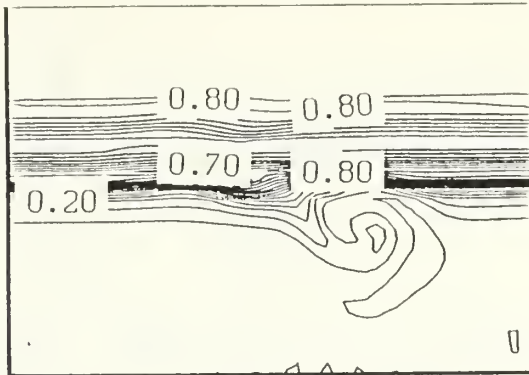


DAY 6

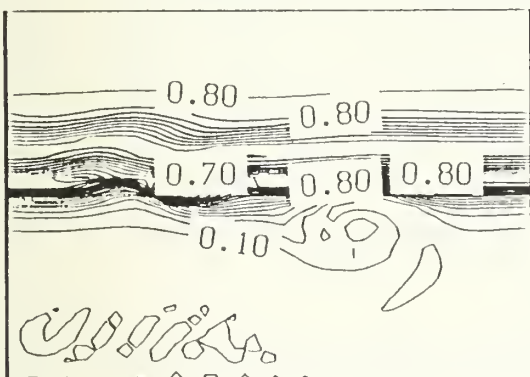
Figure 4.11 Upper Level Relative Vorticity ($\ast 10^{-6}$) Day 1, 2, 4 and 6 (Cyclone-Jet no winds, Experiment 2B) (Contour interval $5.0 \ast 10^{-6}$)



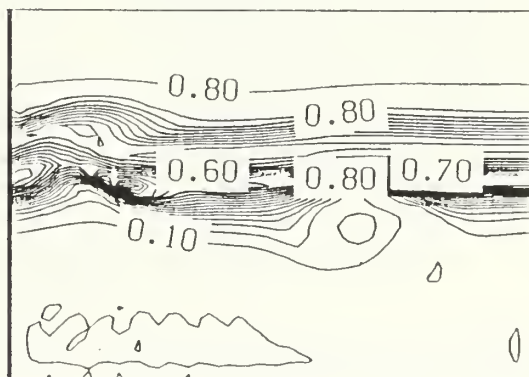
DAY 1



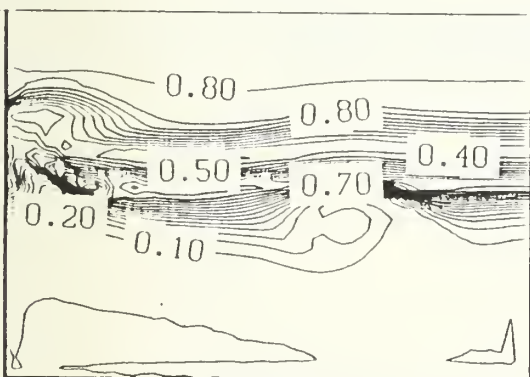
DAY 2



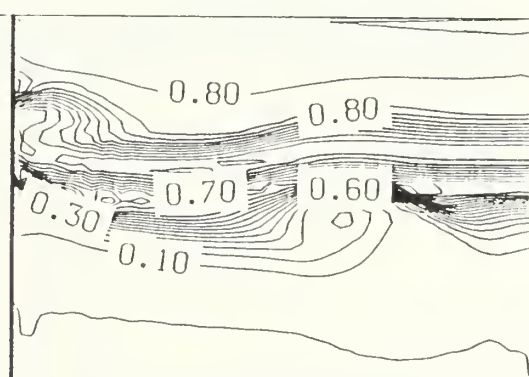
DAY 3



DAY 4

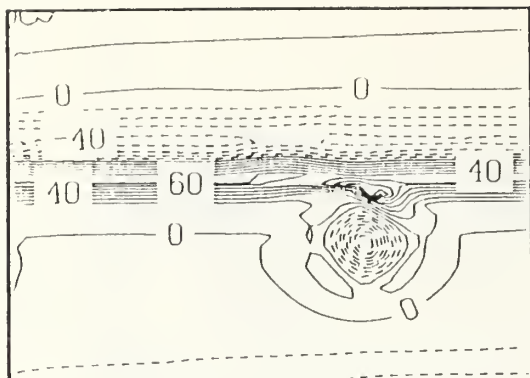


DAY 5

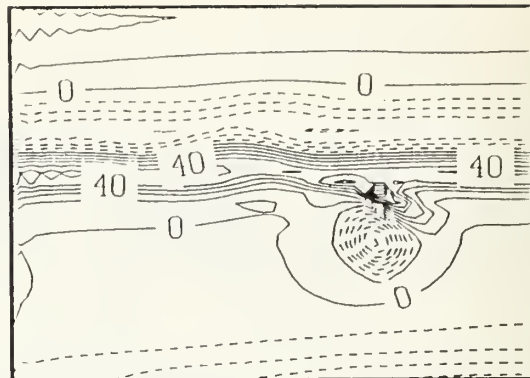


DAY 6

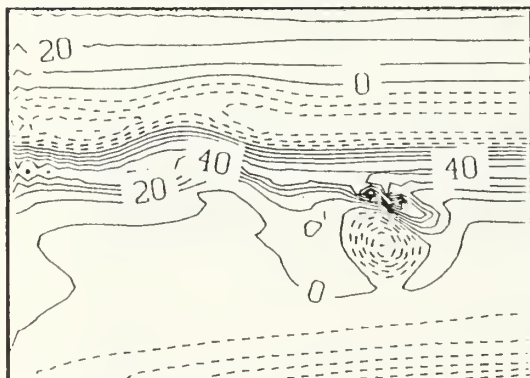
Figure 4.12 Ice Concentration for Day 1-6
(Cyclone-Jet no winds, Experiment 2B)
(Contour interval .05)



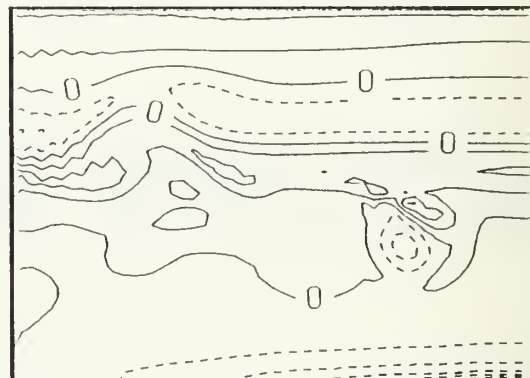
DAY 1



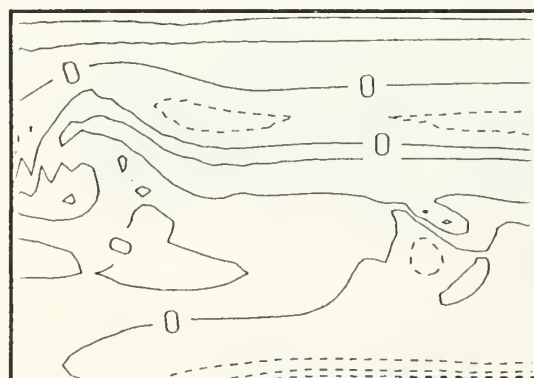
DAY 2



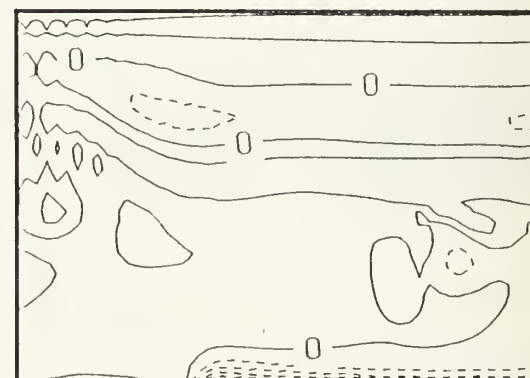
DAY 3



DAY 4

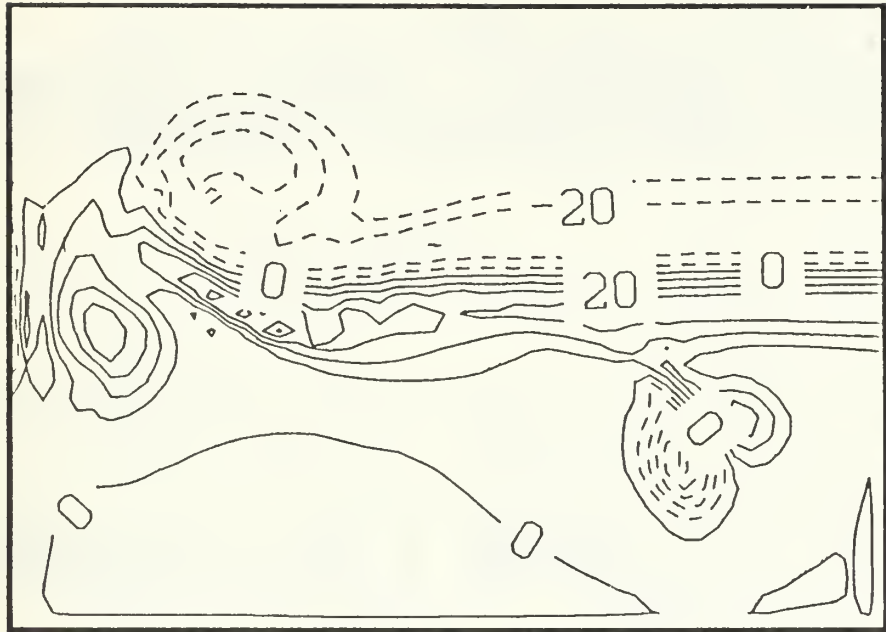


DAY 5



DAY 6

Figure 4.13 Upper Level Relative Vorticity, Day 1-6
(Anticyclone-jet with upwelling winds,
Experiment 3A)



DAY 6

Figure 4.14 Relative Vorticity in the Lower Level,
Day 6 (Anticyclone-jet with upwelling
winds, Experiment 3A)

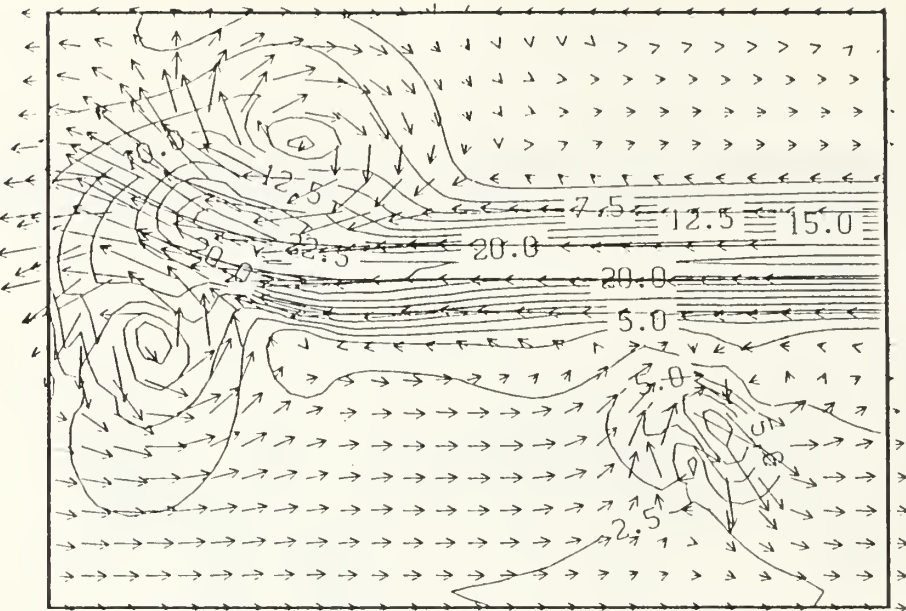


Figure 4.15A Velocity Vectors and Speed Contours (cm/s)
at the Surface Day 6 (Anticyclone-jet no
winds, Experiment 1A) (Contour interval
= 2.5 cm/s)

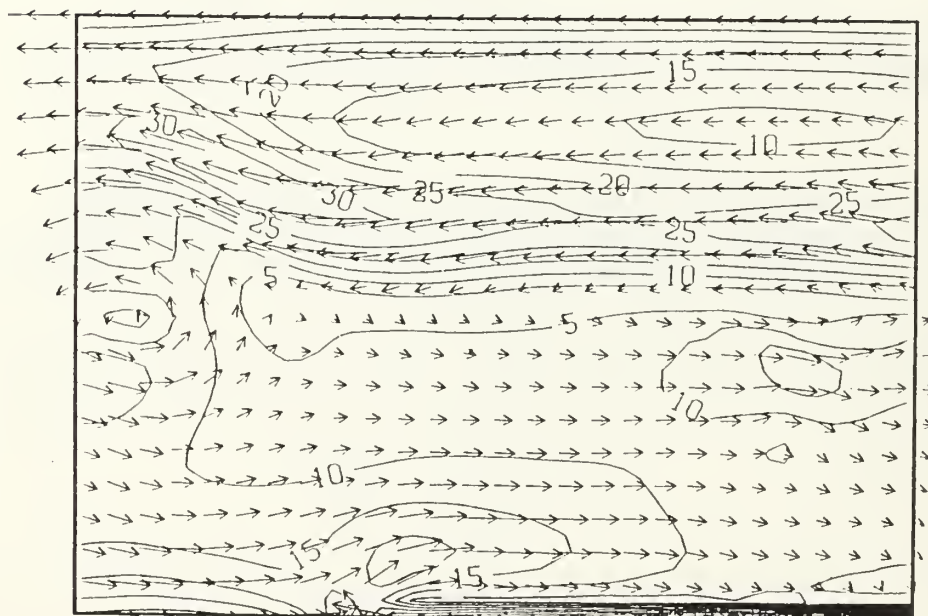
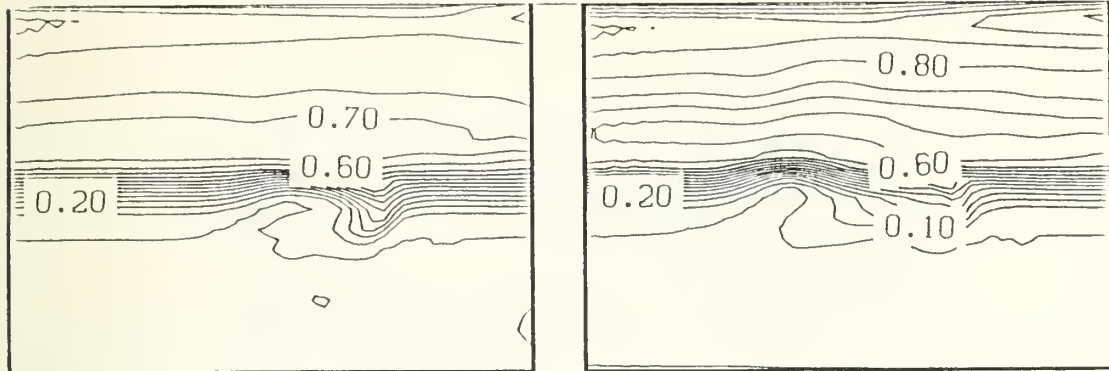
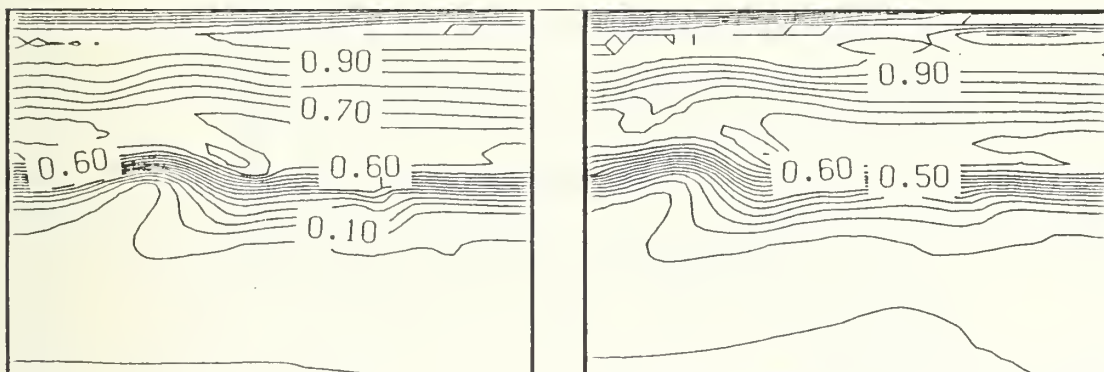


Figure 4.15B Velocity Vectors and Speed Contours (cm/s)
at the Surface Day 6 (Anticyclone-Jet
with upwelling winds, Experiment 3A)
Contour interval = 5 cm/s)



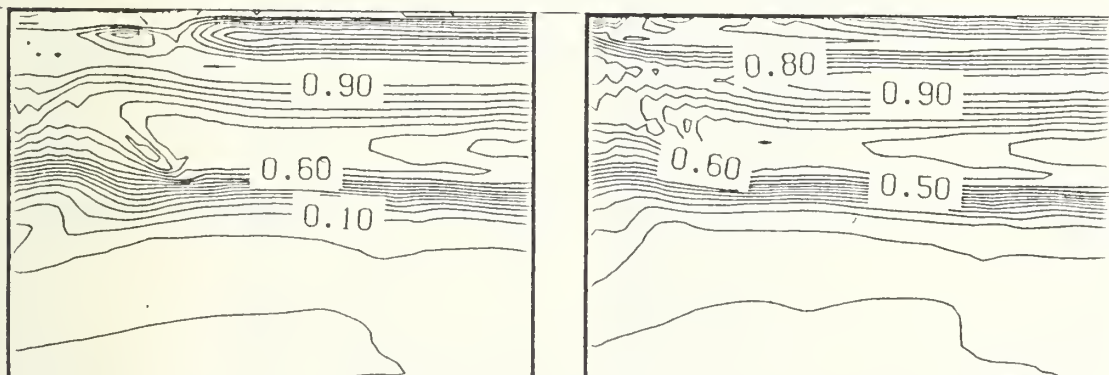
DAY 1

DAY 2



DAY 3

DAY 4



DAY 5

DAY 6

**Figure 4.16 Ice Concentration for Day 1-6
(Anticyclone-Jet with upwelling winds,
Experiment 3A) (Contour interval .05)**

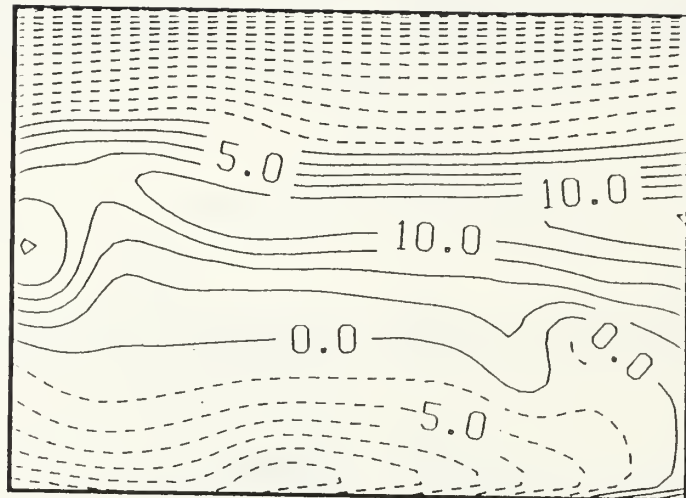


Figure 4.17 Interfacial Height Anomaly (meters) Day 6
 (Anticyclone-Jet with upwelling winds,
 Experiment 3A) (Contour interval = 2.5
 meters)

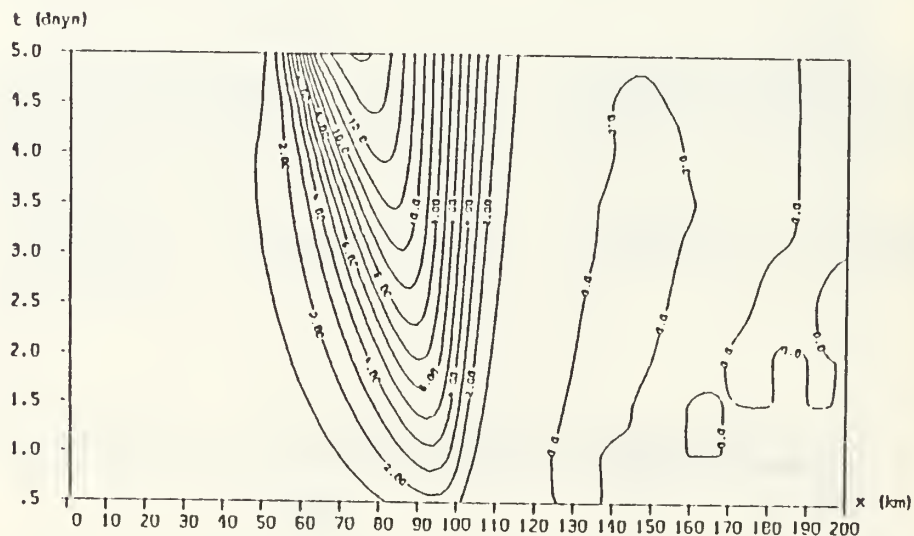


Figure 4.18 x-t plot of Pycnocline Height Anomaly (meters)

Source: Hakkinen (1986b)

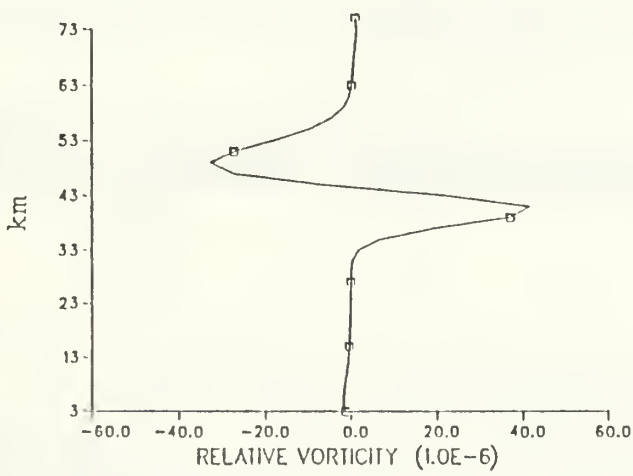


Figure 4.19A Relative Vorticity in the Upper Layer
Across the MIZ, Experiment 1A
Jet/No Eddy/No Wind Day 4 Along I=20

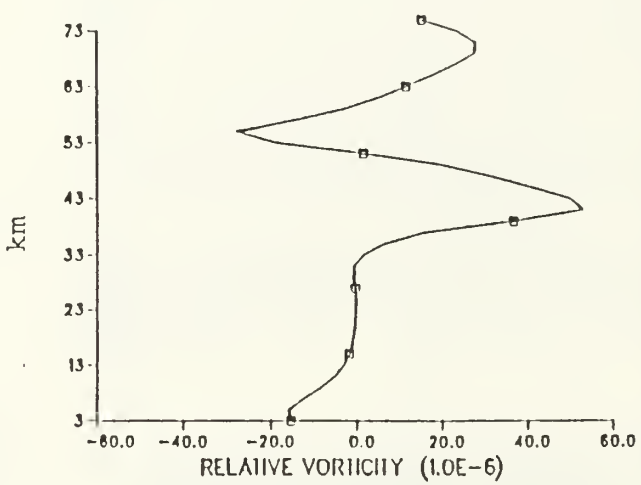
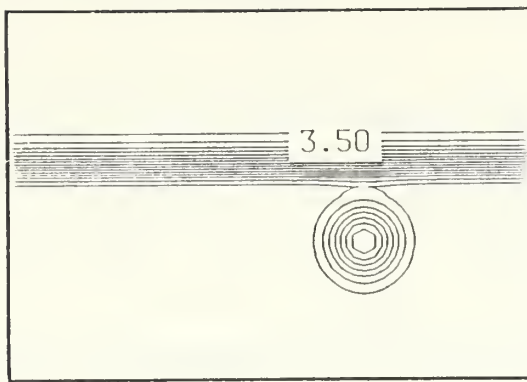
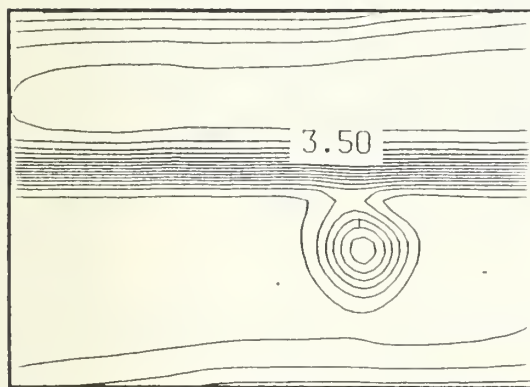


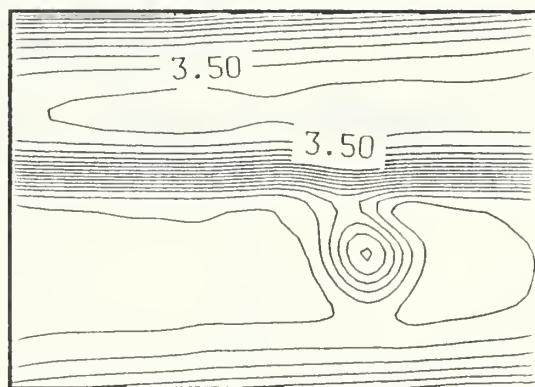
Figure 4.19B Relative Vorticity in the Upper Layer
Across the MIZ, Experiment 2A
Jet/No Eddy/No Wind Day 4 Along I=20



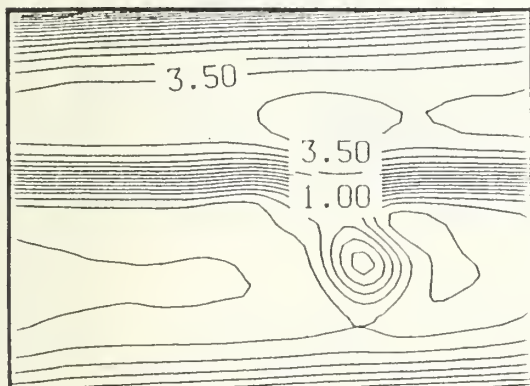
DAY 0.5



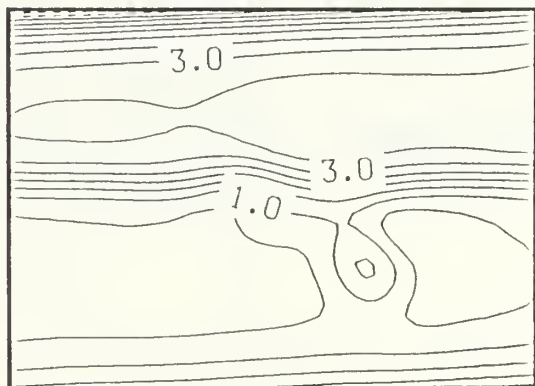
DAY 1



DAY 1.5

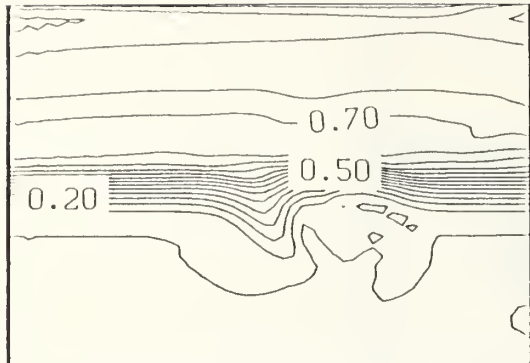


DAY 2

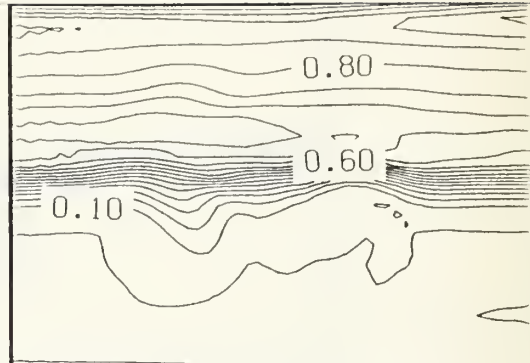


DAY 2.5

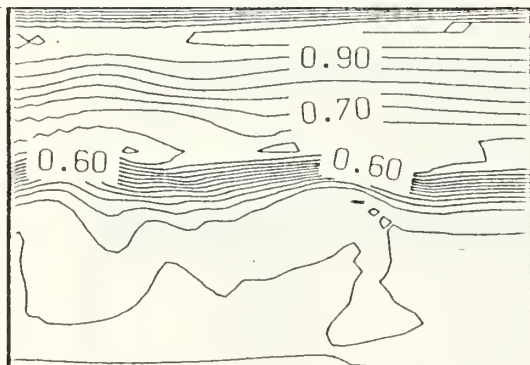
Figure 4.20 Height Anomaly in the Upper Level, Day 0.5 - Day 2.5 (Anticyclone-jet with downwelling winds, Experiment 3B) (Contour interval .5 meters)



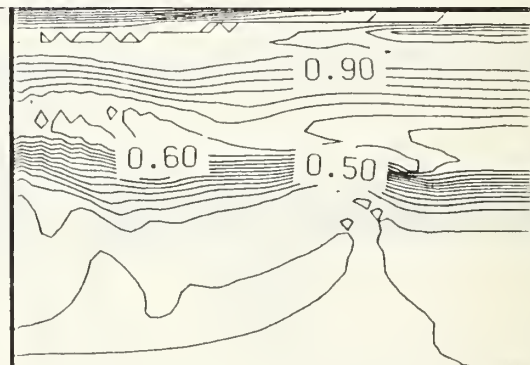
DAY 1



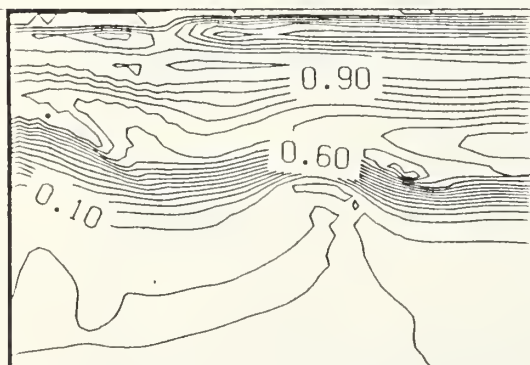
DAY 2



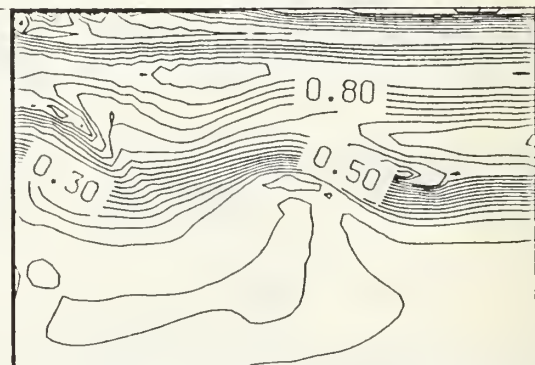
DAY 3



DAY 4

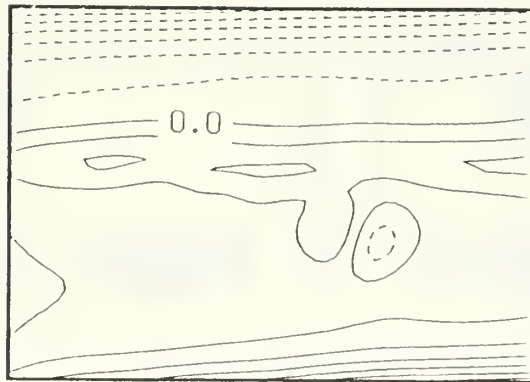


DAY 5

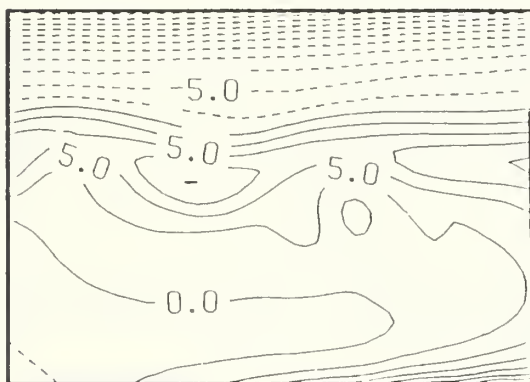


DAY 6

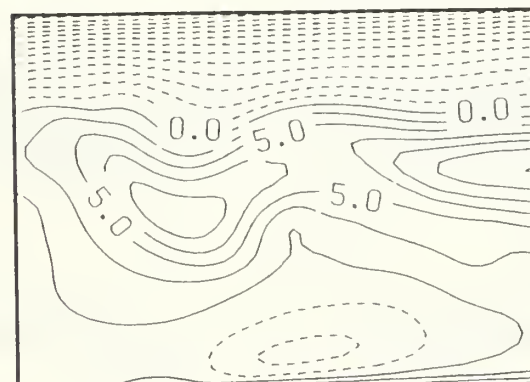
Figure 4.21 Ice Concentration Day 1-6
(Cyclone-Jet with upwelling winds,
Experiment 4A)
(Contour Interval .05)



DAY 2

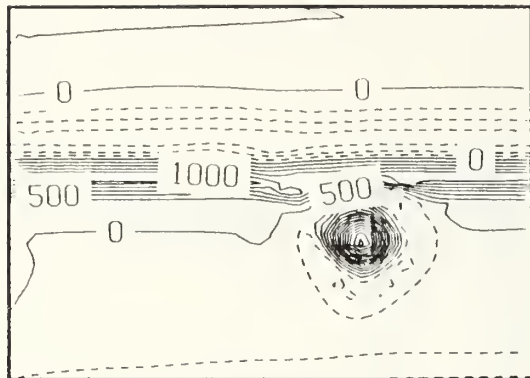


DAY 4

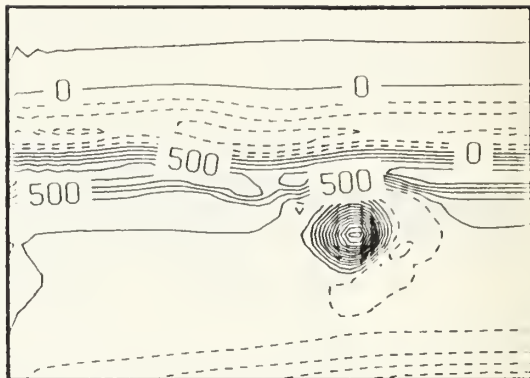


DAY 6

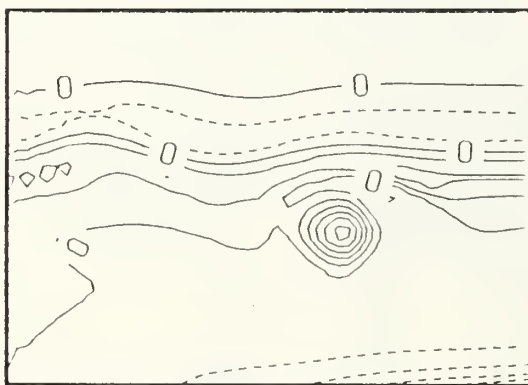
Figure 4.22 Interfacial Height Anomaly, Day 2, 4, & 6
(Cyclone-Jet with upwelling winds,
Experiment 4A)



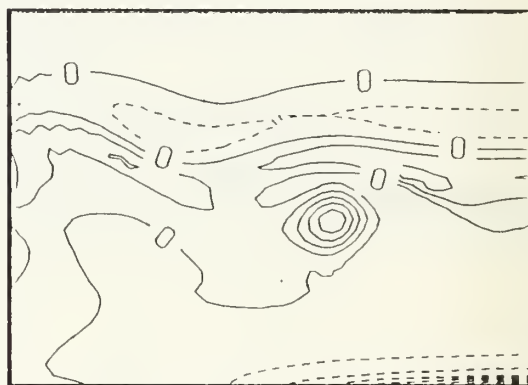
DAY 1



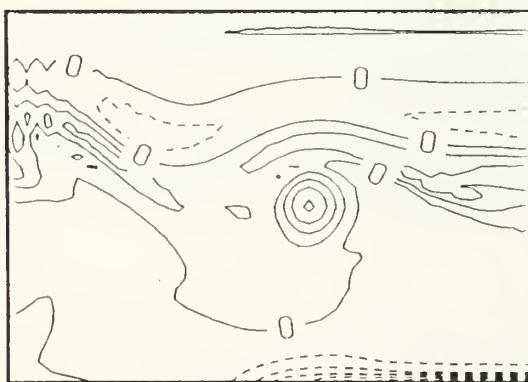
DAY 2



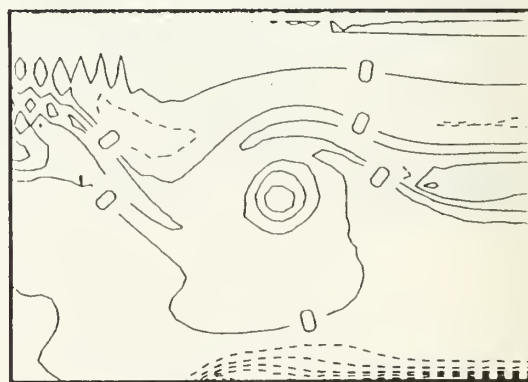
DAY 3



DAY 4

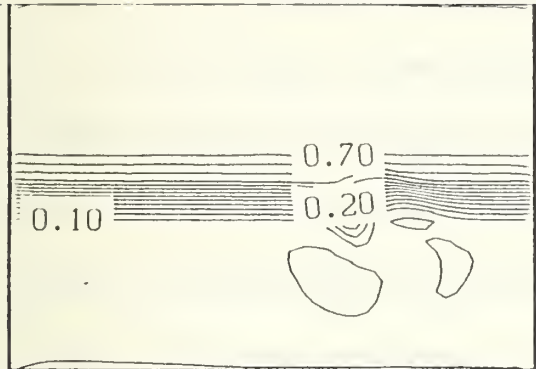


DAY 5

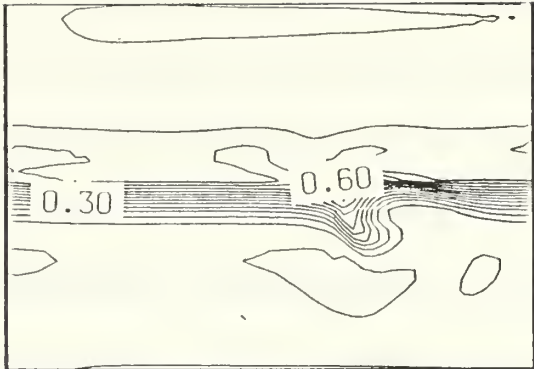


DAY 6

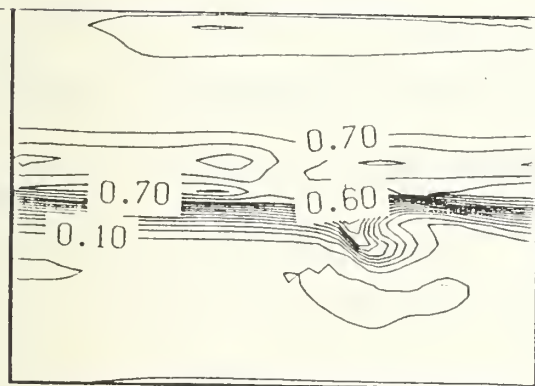
Figure 4.23 Relative Vorticity in the Upper Level,
Day 1-6 (Cyclone-Jet with upwelling winds,
Experiment 4A)



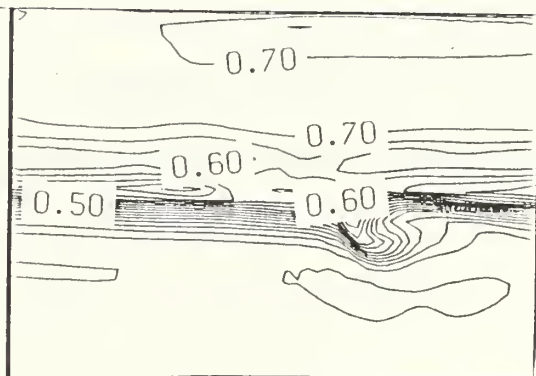
DAY .5



DAY 1



DAY 1.5



DAY 2

Figure 4.24 Ice Concentration Day 1-2
(Cyclone-Jet with downwelling winds,
Experiment 4B) (Contour interval .05)

7. Topography

Many experiments were run using the topographic slope of the East Greenland region to examine the effect of the slope on the eddy-jet interaction. Since the runs were all barotropic, the jet and the eddy interact with the bottom. Most of the effects discussed above are largely unmodified by the inclusion of topography. Dipole formation for an anticyclone-jet interactions can still occur, however, however, there is some evidence of topographic dispersion contributes to the dipole decay. The downstream growth of perturbations in the jet induced by the eddy are less over a sloping bottom. This is consistent with vorticity conservation. The topography thus stabilizes the jet. For the purpose of this study, topography is seen to have no significant effect on the eddy-jet interaction in the upper level.

V. CONCLUSIONS

The East Greenland Current and its associated marginal ice zone is a region of intense circulation. The purpose of this study was to examine the eddy-jet interaction in this region. The understanding of the dynamics of this area and their effects on the ice edge is important to naval operations as well as commercial shipping.

A two layer, primitive equation, numerical model was used to simulate the eddy-jet interaction while varying selected parameters. The effects of wind direction, eddy rotation, and topography on the interaction were examined to determine the dipole formation, seaward ice transport, and icebanding. The model output consists of ice concentration, upper and lower layer relative vorticity, surface height anomaly, and interfacial height anomaly.

Several icebanding mechanisms have been modeled in the past (Hakkinen 1986a) using wind forcing. This study demonstrates how an ocean jet generates an iceband by Ekman transport within one day, while wind forcing generally takes up to twelve days. The eddy interaction with the jet

has no effect on the banding other than to cause it to conform to the sinuous pattern created during the initial interaction.

The development of an ocean dipole is observed in the anticyclone-jet interaction due to the interaction of the anticyclonic vorticity of the eddy interacting with the cyclonic vorticity of the jet. A second smaller eddy develops from the jet and this dipole advects ice away from the ice edge due to the propagation tendency away from the ice edge. The dipole development is not observed in the cyclone-jet interaction case.

The observation of ice tongue formation by Gascard et al. (1988) is also observed in the experiment involving the interaction of an anticyclone-jet with no winds. On day six there is a substantial ice tongue developing from an originally straight ice edge due to the perturbation of the jet by the anticyclone. The ice tongue has anticyclonic curvature, curving toward the downstream boundary. Another experiment in which there was ice tongue development was the cyclone-jet interaction with downwelling winds. Although the ice tongue is not as pronounced, it is interesting to note that the ice tongue

has cyclonic curvature toward the upstream boundary. It was seen that the interaction of a eddy and a jet perturbs the ice edge and the perturbation was advected downstream. The distance between ice edge perturbations is approximately 80-90 km, similar to that observed by Gascard et al. (1988). It should be noted that the model has a constant jet velocity of 30 cm/s while the East Greenland current is a variable 30-40 cm/s, Gascard et al. (1988). The interaction of an eddy with a jet in the marginal ice zone is also important in that it is a mechanism for the formation of a sinuous ice edge. The sinuous ice edge is shown to favor wind generation of ice edge eddies through differential Ekman pumping (Hakkinen, 1986b). This is observed in the experiments with upwelling favorable winds.

Winds perform an important role in the dynamics of the eddy-jet interaction. The important conclusion is that the winds 10 m/s or greater dominate ice dynamics in the upper layer. In both the anticyclone and cyclone-jet interaction with winds of 10 cm/s the ice edge becomes less sinuous. While dipole formation can still occur in the case of anticyclone-jet interaction with upwelling winds,

there is no ice export seaward suggesting that dipole events seen in SAR imagery are most likely from light wind periods. The upwelling and downwelling band development from along ice winds is observed in the wind experiments. This supports the upwelling and downwelling along ice theory of Hakkinen (1986b).

The same experiments conducted with a flat bottom were repeated using a linearly sloping bottom to a maximum depth 4010 meters, simulating the East Greenland ocean topography. Topographic dipole formation and dispersion in the interfacial height anomaly are observed but the effect of topography on the eddy-jet interaction was small.

VI. RECOMMENDATIONS

Observations have shown that the East Greenland Current has substantial vertical shear. Since this study evaluates the effects of a barotropic eddy-jet interaction in the marginal ice zone, it would provide a good basis for a follow on study for a barotropic eddy interaction with a baroclinic jet.

Additional experiments with a more realistic bottom topography of the region should be conducted to examine the effects of the bottom topography in a baroclinic jet barotropic eddy interaction. Time dependent, off ice edge winds should also be included in the study to simulate those winds observed by Johannessen et al. (1987) (Figure 4.1) to examine their effects on icebanding. Similar experiments using a larger domain to eliminate the effect of the artificial jet on the dipole formation should be examined.

APPENDIX

SYMBOLS AND NOTATION

A	Ice Concentration	
A _e	Eddy maximum amplitude	
A _a	Laplacian lateral friction coefficient for ice concentration	= 30
A _h	Laplacian lateral friction coefficient	= 10m ² /s
A _j	Jet maximum amplitude	= .04 m ²
A _m	Laplacian lateral friction coefficient for ice mass	= 30
B	Variation of Coriolis parameter with latitude	= 3.8 x 10 ⁻¹² m ⁻¹ /s ⁻¹
c _{ai}	Air-ice interfacial stress coefficient	= 2.5 x 10 ⁻³
c _{aw}	Air-water interfacial stress coefficient	= 1.4 x 10 ⁻³
c _{iw}	Ice-water interfacial stress coefficient	= 7.5 x 10 ⁻³
c	Phase speed of perturbation wave	= m/s
D	Ice thickness distribution	= m/ $\rho_i A$
Δx	Grid spatial resolution	= 1.0 km
Δt	Time increment	= 600 s

δ_{ii}	Kronecker delta function	= 0 when $i=2$
f_0	Coriolis parameter for mean latitude	= $1.43 \times 10^{-4} \text{ s}^{-1}$
g	Gravitational acceleration	= 9.8 m/s^2
	Nondimensional eddy size	= L/R_d
H_1	Upper layer mean thickness	= 50 m
H_2	Lower layer mean thickness	= 4000 m
h_i	Instantaneous layer thickness	= 50 m
L_e	e-folding scale of the ocean eddy	= 5 km
L_j	e-folding scale of the ocean jet	= 5 km
m	Ice mass per unit area	= kg/m^2
P_1	Pressure in the upper layer	= $g(h_1+h_2+d)$
P_2	Pressure in the lower layer	= $P_1 - g' h_1$
Q	Nondimensional eddy strength	= $v_{\max}/\beta R_d^2$
q_i	upper, lower layer potential vorticity	= $\frac{f + \zeta}{h_i}$
R_d	First internal Rossby radius of deformation	= $[g' H_1 H_2 / f_0^2 (H_1 + H_2)]^{1/2}$
R_o	Rossby number	= v_{\max}/fL
ρ_a	Density of air	= 1 kg m^{-3}
ρ_i	Density of ice	= 910 kg m^{-3}
τ^{ai}	Air-ice interfacial stress vector	
τ^{iw}	Air-water interfacial stress vector	
τ^{aw}	Ice-water interfacial stress vector	

v_{\max} Eddy maximum tangential vector = 15 cm/s⁻¹

x, y Cartesian coordinates directed
N and W respectively

ζ_1 Upper, lower layer relative
vorticity = $\nabla \times v_1$

∇ Gradient operator = $\frac{\partial}{\partial x} + \frac{\partial}{\partial y}$

∇^2 Laplacian operator = $\frac{\partial^2}{\partial x^2} + \frac{\partial^2}{\partial y^2}$

LIST OF REFERENCES

Camerlengo, A., and O'Brien, J.J., "Open Boundary Conditions in Rotating Fluids," *Journal of Computational Physics*, v. 35, pp. 12-35, 1980.

Foldvik, A, Aagaard, K., and Torresen, T., "On the Velocity Field of the East Greenland Current," *Deep Sea Research*, v. 35, no. 8, pp. 1335-1354, 1988.

Gascard, J.C., Kergomard, C., Jeannin, P. F., and Fily, M., "Diagnostic Study of the Fram Strait Marginal Ice Zone During Summer From 1983 and 1984 Marginal Ice Zone Experiment Lagrangian Observations," *Journal of Geophysical Research*, v. 93, pp. 3613-3641, 1988.

Hakkinen, S., "Ice Banding in the Coupled Ice-Ocean," *Journal of Geophysical Research*, v. 91, pp. 5047-5053, 1986a.

Hakkinen, S., "Coupled Ice-Ocean Dynamics in the Marginal Ice Zones: Upwelling/Downwelling and Eddy Generation," *Journal of Geophysical Research*, v. 91, pp. 819-832, 1986b.

Hibler, W. D. III, "A Dynamic Thermodynamic Sea Ice Model," *Journal of Physical Oceanography*, v. 9, pp. 815-846, 1979.

Hibler, W. D. III, "Ice Dynamics", CRREL Monogr. 84-3, U.S. Army Cold Regions Research and Engineering Laboratory, Hanover, N.H., 1984.

Hurlburt, H.E., and Thompson J. D., "A Numerical Study of Loop Current Intrusions and Eddy Shedding," *Journal of Physical Oceanography*, v. 9, pp. 1611-1651, 1980.

Johannessen, O.M., Johannessen, J.A., Morison, J., Farrelly B.A., Svendsen E.A.S., "Oceanographic Conditions in the Marginal Ice Zone North of Svalbard in Early Fall 1979 with an Emphasis on Mesoscale Processes," *Journal of Geophysical Research*, v. 88, pp. 2755-2769, 1983.

Johannessen, J.A., Johannessen, O.M., Svendsen E., Shuchman, R., Manley, T., Campbell, W., Josberger, E., Sandven, S., Gascard, J.C., Olaussen, T., Davidson, K., and Van Leer, J., "Mesoscale Eddies in the Fram Strait Marginal Ice Zone During MIZEX 1983 and 1984," *Journal of Geophysical Research*, v. 92, pp. 6754-6772, 1987.

Paquette, R.G., Bourke R.H., Newton, J.F., Perdue, W.F., "The East Greenland Polar Front in Autumn," *Journal of Geophysical Research*, v. 90, pp. 4866-4882, 1985.

Shuchman, R.A., Sutherland L.L., and Burns, B.A., *MIZEX 1987 SAR Data Summary*, 1988.

Smedstad, O.M. and Roed, L.P., "A Coupled Ice-Ocean Model of Ice Breakup and Banding in the Marginal Ice Zone," *Journal of Geophysical Research*, v. 90, pp. 876-882, 1987.

Smith, D.C., IV, Bird, A., and Budgell, W.P., "A Numerical Study of Mesoscale Ocean Eddy Interaction with a Marginal Ice Zone," *Journal of Geophysical Research*, v. 93, no.12, pp. 461-12, 473, 1988.

Smith, D.C. IV, Davis, G.P., "A Numerical Study of Eddy Interaction with an Ocean Jet," accepted by *Journal of Physical Oceanography*, Feb. 1989.

Smith, D.C. IV, and O'Brien, J.J., "The Interaction of a Two-Layer Isolated Mesoscale Eddy with Topography," *Journal of Physical Oceanography*, v. 13, pp. 1681-1697, 1983.

Smith, D.C. IV, and Reid R.O., "A Numerical Study of Nonfrictional Decay of Mesoscale Eddies," *Journal of Physical Oceanography*, v. 12, pp. 244-255, 1982.

Stern, M. and Flierl, G.R., "On the Interaction of a Vortex with a Shear Flow," *Journal of Geophysical Research*, v. 92, no. 10, pp. 733-10, 744, 1987.

INITIAL DISTRIBUTION LIST

	No. Copies
1. Defense Technical Information Center Cameron Station Alexandria, VA 22304-6145	2
2. Library, Code 0142 Naval Postgraduate School Monterey, CA 93943-5002	2
3. Chairman, Code 63Rd Department of Meteorology Naval Postgraduate School Monterey, CA 93943	1
4. Chairman, Code 68Co Department of Oceanography Naval Postgraduate School Monterey, CA 93943	1
5. Professor David C. Smith IV, Code 68Si Department of Oceanography Naval Postgraduate School Monterey, CA 93943	3
6. Professor J.C. Gascard Department of Oceanography Naval Postgraduate School Monterey, CA 93943	1
7. Director Naval Oceanography Division Naval Observatory 34 th and Massachusetts Avenue NW Washington, DC 20390	1

8. Commander	1
Naval Oceanography Command	
NSTL Station	
Bay St Louis, MS 39522	
9. Commanding Officer	2
Naval Oceanographic Office	
NSTL Station	
Bay St Louis, MS 39522	
10. Commanding Officer	1
Fleet Numerical Oceanography Center	
Monterey, CA 93943	
11. Commanding Officer	1
Naval Ocean Research and Development Activity	
NSTL Station	
Bay St Louis, MS 39522	
12. Commanding Officer	1
Naval Environmental Prediction Research Facility	
Monterey, CA 93943	
13. Chairman, Oceanography Department	1
U.S. Naval Academy	
Annapolis, MD 21402	
14. Chief of Naval Research	1
800 North Quincy Street	
Arlington, VA 22217	
15. Office of Naval Research, Code 420	1
Naval Ocean Research and Development Activity	
800 North Quincy Street	
Arlington, VA 22217	
16. Scientific Liaison Office	1
Office of Naval Research	
Scripps Institution of Oceanography	
La Jolla, CA 92037	

17. Chief, Ocean Services Division National Oceanic and Atmospheric Administration 8060 Thirteenth Street Silver Spring, MD 20910	1
18. Professor R. Bourke, Code 68Pa Department of Oceanography Naval Postgraduate School Monterey, CA 93943	1
19. Commanding Officer Naval Polar Oceanographic Center 4301 Suitland Road Washington, DC 20390	1
20. LT Rutledge P. Lumpkin Rt 2 Box 175 Georgetown, SC 29440	3

Thesis ✓
L8953 Lumpkin
c.1 A numerical study of a
mesoscale eddy inter-
action with an ocean
front in the marginal
ice zone.

Thesis
L8953 Lumpkin
c.1 A numerical study of a
mesoscale eddy inter-
action with an ocean
front in the marginal
ice zone.



thesL8953
A numerical study of a mesoscale eddy in



3 2768 000 81782 9

DUDLEY KNOX LIBRARY